Peer-reviewed version available at *Biomolecules* **2020**, *10*, 479; doi:10.3390/biom10030479

1*H*-Imidazole-2,5-Dicarboxamides as NS4A Peptidomimetics: Identification of a New Venue to Inhibit HCV-NS3 Protease

Abdelsattar M. Omar[a,b], Mahmoud A. Elfaky[c], Stefan T. Arold[d], Sameh H. Soror[e,f], Maan T. Khayat[a], Hani Z. Asfour[g], Faida H. Bamane[h] and Moustafa E. El-Araby[a]*

[a] *Department of Pharmaceutical Chemistry, Faculty of Pharmacy, King Abdulaziz University, Alsulaymanyah, Jeddah 21589, Saudi Arabia*

[b] *Department of Pharmaceutical Chemistry, Faculty of Pharmacy, Al-Azhar University, Cairo, Egypt*

[c] *Department of Natural Products and Alternative Medicine, Faculty of Pharmacy, King Abdulaziz University, Alsulaymanyah, Jeddah 21589, Saudi Arabia*

[d] *Computational Bioscience Research Center, Division of Biological and Environmental Sciences and Engineering, King Abdullah University of Science and Technology, Thuwal, Saudi Arabia*

[e] *Center for Scientific Excellence Helwan Structural Biology Research (HSBR), Faculty of Pharmacy, Helwan University, Ain Helwan, P.O. 11795, Cairo, Egypt*

[f] *Department of Biochemistry and Molecular Biology, Faculty of Pharmacy, Helwan University, Ain Helwan, P.O. 11795, Cairo, Egypt*

[g] *Department of Medical Microbiology and Parasitology, Faculty of Medicine, King Abdulaziz University, Jeddah 21589, Saudi Arabia*

[h] *Department of Biochemistry, Faculty of Medicine, King Abdulaziz University, Jeddah 21589, Saudi Arabia*

*Corresponding Author: Moustafa E. El-Araby. *Address*: Bldg. 6, Faculty of Pharmacy, Office 642/2, Almalaeb street, King Abdulaziz University, Alsulaymanyah, Jeddah 21589, Saudi Arabia. *E-Mail Address*: madaoud@kau.edu.sa

ABSTRACT

The non-structural protein NS3/4A protease is a critical factor for hepatitis C virus (HCV) maturation that requires activation by NS4A. Synthetic peptide mutants of NS4A were found to inhibit NS3 function. The bridging from peptide inhibitors to heterocyclic peptidomimetics of NS4A has not been in consideration in literature, and therefore, we decided to explore this strategy to develop a new class of NS3 inhibitors. In this report, a structure-based design approach was used to convert the bound form of NS4A into 1*H*-imidazole-2,5-dicarboxamide derivatives as first generation peptidomimetics. This scaffold mimics the buried amino acid sequence Ile-25` to Arg-28` at the core of $NS4A_{21`-33`}$ needed to activate the NS3 protease. Some of the synthesized MOC compounds were able to compete with and displace $NS4A_{21`-33`}$ for binding to NS3. For instance, N^5-(4-guanidinobutyl)-N^2-(*n*-hexyl)-1*H*-imidazole-2,5-dicarboxamide (MOC-24) inhibited the binding of $NS4A_{21`-33`}$ with a competition IC_{50} of 1.9 ± 0.12 µM in a fluorescence anisotropy assay, stabilized the denaturation of NS3 by increasing the aggregation temperature by ΔT_{agg} 0.6 ± 0.140 °C. MOC-24 also inhibited NS3 protease activity in a fluorometric assay. Molecular dynamics simulations rationalized the structure-activity relationship (SAR) differences between the active MOC-24 and the inactive MOC-26. Our data shows that MOC compounds are possibly the first examples of NS4A peptidomimetics that demonstrated promising activities against NS3 proteins.

Keywords: NS3 inhibitors; allosteric inhibitors; NS4A; peptidomimetics; imidazole; hepatitis C virus; molecular dynamics; *Flaviviridae*; DSLS; binding assay.

INTRODUCTION

Peer-reviewed version available at *Biomolecules* **2020**, *10*, 479; doi:10.3390/biom10030479

Hepatitis C is a life-threatening, wide spread viral infection [1]. Initially, the virus infects liver cells but remains asymptomatic for extended periods. This invisibility constitutes epidemiological challenges because patients diagnosed with hepatitis C come from two pools; recently-infected and late-stage asymptomatic. The initial symptoms such as fever, fatigue, nausea and liver tenderness can be misleading because they are tolerated by most of patients. After several years of this blood-borne infection, the virus activates, replicates, and causes complications that start with liver scarring, fibrosis followed by cirrhosis and eventually liver failure and carcinoma [2,3]. Awareness of hepatitis C health problems and forceful efforts to combat the spread of HCV in healthcare settings have led to a significant decline in new hepatitis C cases. However, the death toll from complications of this disease remains as high as 400,000 annually due to the above described unique clinical *vs.* epidemic profile of the chronic hepatitis C. An estimated 70 million people globally are currently infected with HCV, constituting a major health problem [1]. In 2013, the death rate from HCV complications surpassed that of HIV. In 2015, hepatitis C-related deaths exceeded that of tuberculosis and malaria combined [4].

Up until 2013, interferon (or pegylated interferon) and ribavirin were the most effective available therapies, but their long-term efficacies were as low as 3% [5]. Identification of the hepatitis C genome-proteome in early 1990s prompted intensive research that led to the introduction of the new class of direct antiviral agents (DAAs). DAAs revolutionized the treatment of hepatitis C and succeeded to control the global crisis of this epidemic that was once described as “Third Millennium Challenge” [2]. Recently, combinations of DAAs have become an effective way to cover hepatitis C infection of different genotypes [6,7]. Nonetheless, according to the World Health Organization, there

are several remaining challenges that must be met to eradicate HCV [1]; 1) Access to the treatment in economically-challenged areas must be increased [8]; 2) Emerging drug resistance is an expected problem even with combination therapy [9,10]; 3) Efficacy in broader sectors of HCV patients, such as elder, impaired kidney and liver patients [11]. Thus, there is a clear need to identify new approaches to inhibit viral targets and to increase the DAA arsenal [12].

The HCV genome is a positive-sense, single-stranded RNA virus belonging to *Flaviviridae* [13]. The virus genome translates mainly to structural and non-structural proteins. The non-structural (NS) proteins include NS3, NS4A, NS4B, NS5A and NS5B and they comprise factors essential for maturation and replication of the virus [14]. NS3 dually functions as a protease (N-terminal domain) and an RNA helicase (C-terminal domain) [15]. When activated as protease, it catalyzes the processing of the viral proteome to functional proteins by cleaving NS3-NS4A, NS4A-NS4B, NS4B-NS5A and NS5A-NS5B junctions. The proper folding of NS3 is indispensable for protease activity and occurs only when it binds to NS4A, a 54 amino acid peptide with multiple functions. NS4A is not only required for NS3 activation [16,17], but it is also important for the integration of the NS3 to the host cell endoplasmic reticulum [18] and for neutralizing host cells immune responses [19,20]. The NS3/4A protease was the first and foremost targeted viral protein with DAAs that bind to its substrate site [21]. Interference with NS4A binding site, on the other hand, has not been evaluated thoroughly as a mechanism to allosterically inhibit the NS3 protein, especially by drug-like peptidomimetics. In this research, we are introducing compounds that were designed to compete and replace NS4A on its NS3 binding site leading to NS3 inhibition [22].

2. RESULTS

2.1. Rationale and Design

The NS4A N-terminal intercalates between the β-strands A0 and A1 (the first 28 residues of the N-terminal) of NS3. The association with NS4A induces proper conformation of the apoenzyme and increases the proteolytic activity of NS3 by ~950 times [14,16,23]. Accumulated evidences established that the central region of NS4A (Gly21`-Leu32`) is sufficient for activation of the NS3 protease [24-27]*. It has been also confirmed by our laboratory [28,29] and others [26,30] that certain mutants can bind to the NS4A site and inhibit the protease function of NS3. In their reporting of the first crystal structure of NS3/4A, Kim and coworkers, stated that "The contact surface between NS3 and NS4A is quite extensive and provides another possible site for the design of anti-HCV chemotherapeutic agents" [14]. However, subsequent research focused merely on the discovery of NS3/4A substrate site inhibitors, while the NS4A site inhibitors were rarely mentioned in few reports as a hypothetical approach [14,31,32]. Accordingly, we decided to pursue this concept by designing peptidomimetics that bind and replace NS4A on the protease domain of NS3.

We started the *de novo* design of NS4A peptidomimetics by inspection of the crystal structures of NS3-NS4A complexes (PDB Code: 1NS3) [23]. We noticed that NS4A forms a β-stand that is mostly extended, except in a turn (kink) featuring a nearly planar area. This planar kink is composed of one eclipsed *cis* bond with a dihedral angle of -12º (the negative sign denotes a deviation to the opposite side of the Val-26` side chain) and four

* the prime (`) mark was given throughout this article to differentiate between residues of NS4A from that of NS3 apoenzyme

near perfect planar *trans* bonds spanning through Val-26` to Arg-28` (Figure 1A, torsion table in Supplementary Material Table S1-A). This *cis* bond largely depends on the presence of Gly-27` because it allows lessening the steric conflict with the Val-26`side chain. Interestingly, this glycine turn is conserved in all crystal structures of HCV NS3 protease deposited to date in the Protein Data Bank (PDB), regardless of their genotype [33-35] or of the sequence constructs used (NS4A fused with NS3 or non-fused) [14,23,35] (See Supplementary Material, Figure S1-A). Accordingly, we postulated that an imidazole nucleus appending two amide groups should mimic this planar region. Docking experiments by manual "visually guided" methods suggested that the 1*H*-imidazole-2,5-dicarboxamide nucleus can occupy the planar region while keeping key interactions of NS4A in place without posing significant steric conflicts (Figure 1B). In particular, the N1 of the imidazole acted as a hydrogen bond donor with the backbone carbonyl of Ile-35 (located in the A1 β-sheet), which also made a hydrogen bonding with CO of the 5-carboxamide group of the designed scaffold. The carbonyl of the C2-carboxamide group occupied a planar area in which Val-26` rests. In previous studies, Val-26` side chain deemed unnecessary for NS4A function and therefore, could be safely replaced by the intended amidic carbonyl [26]. The pocket accommodating Ile-25` hydrophobic side chain has been sought as an opportunity to increase the binding potency of our compounds. In the context of probing this hydrophobic pocket, we decided to synthesize compounds of different hydrophobic substituents at the C2 amide group. The imidazole's C5 carboxamide occupied the same position of the amide bond between Gly-27` and Arg-28` conserving a hydrogen bond with Gln-8 (located within the A0 sheet). Its agmantyl substituents occupied the same position of Arg-28` side chain. In addition, the bifurcate hydrogen

Preprints (www.preprints.org) | NOT PEER-REVIEWED | Posted: 24 January 2020 doi:10.20944/preprints202001.0279.v1

Peer-reviewed version available at Biomolecules 2020, 10, 479; doi:10.3390/biom10030479

bonding between the backbone carbonyl of Val-26` and NH's of Thr-10 and Arg-11 were compensated by hydrogen bonding accepted by the N3 of the 1*H*-imidazole core (Figure 2).

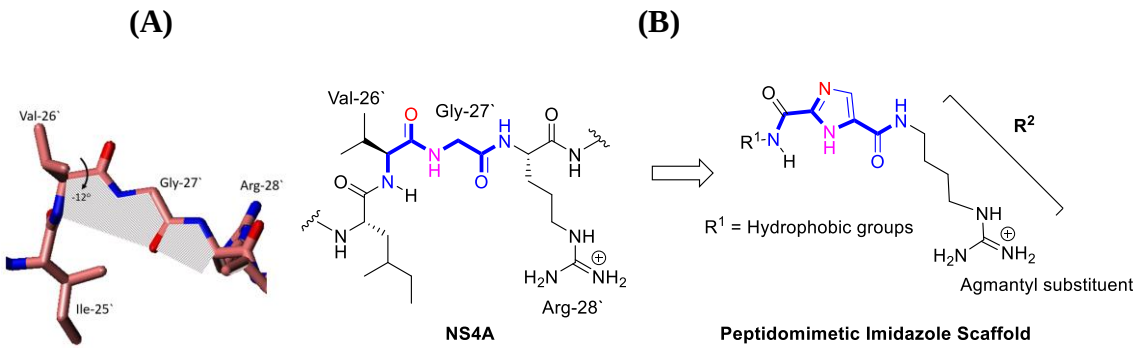

Figure 1. (A) The planar kink region of NS4A extracted from crystal structure 1NS3 (PDB Code: 1NS3) is shadowed. (B) *De novo* design of 1*H*-imidazole-2,5-diamide derivatives that mimic this planar area.

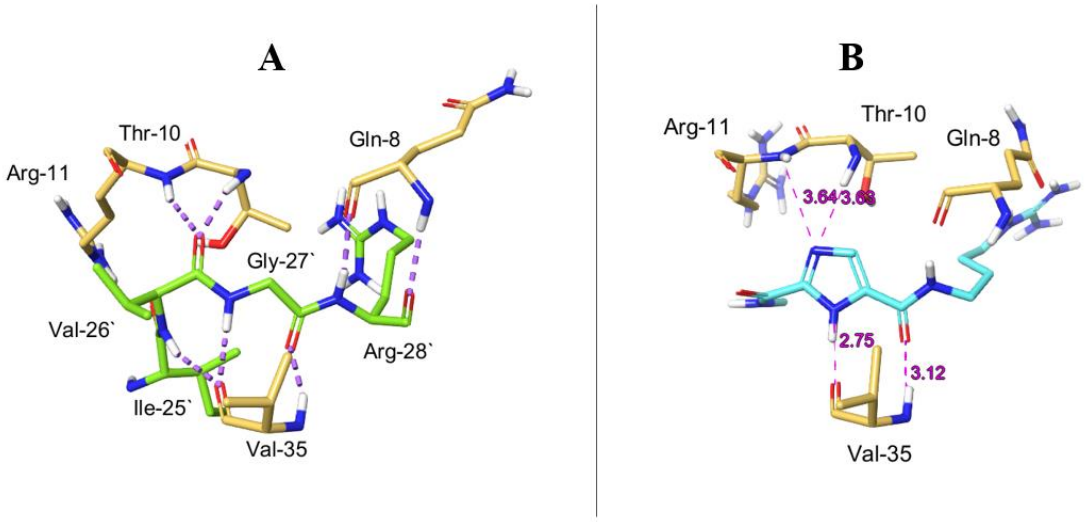

Figure 2. Conservation of important hydrogen bonding in the structure-based design. (A) Interactions of NS4A (light green) with some NS3 residues (yellow). (B) Designed Imidazole-2,5-dicarboxamide (light blue).

2.3. Synthesis of 1*H*-imidazole-2,5-dicarboxamide derivatives

The final MOC† compounds were synthesized using reported chemistry [36-39] as illustrated in the synthetic scheme 1. Starting from cyanoformic acid ethyl ester (**1**), the

† MOC is a project code and therefore, final compound coding is not necessarily sequential not starting from MOC-1.

nitrile group was converted to *N*-hydroxyamidino derivative **2** by nucleophilic addition of hydroxylamine [38]. The pivotal imidazole intermediate **3** was prepared by thermal microwave (MW) irradiation-induced cyclo-condensation of **2** with *tert*-butyl propiolate [36,37]. This compound featured the desired imidazole nucleus containing two different ester groups: ethyl (alkali labile) and *t*-butyl (acid labile). Therefore, a trifluoroacetic acid (TFA) treatment could selectively hydrolyze the *tert*-butyl ester to imidazole-5-carboxylic acid **4**. The carboxylic acid was reacted with selected amines of R^2 substituents under catalysis of 1-Ethyl-3-(3-dimethylaminopropyl)carbodiimide (EDCI)/1-hydroxybenzotriazole hydrate (HOBt) to give the intermediates **5a-c**. The ethyl esters **5a-c** were hydrolyzed using LiOH to the lithium salts **6a-c**. The final compounds were obtained from **6a-c** by coupling with the desired amines (R^1-NH_2) under the effect of propylphosphonic anhydride (T3P). The previous amide coupling step of **5a** (R^2 = 2-(methylamino)-2-oxoethyl) and **5b** (R^2 = 2-pyridylmethyl) provided MOC-11 (R^1 = *n*-pentyl) and MOC-33 (R^1 = *n*-hexyl), respectively. The intermediate **5c** (R^2 =diBoc-agmantyl, Boc = *tert*-butoxycarbonyl) [39] resulted in intermediates **7a-i** which were directly subjected to acidic conditions for Boc deprotection to obtain MOC final compounds 23, 24, 26, 27, 28, 29, 30, 31 and 32.

Preprints (www.preprints.org) | NOT PEER-REVIEWED | Posted: 24 January 2020 doi:10.20944/preprints202001.0279.v1

Peer-reviewed version available at Biomolecules 2020, 10, 479; doi:10.3390/biom10030479

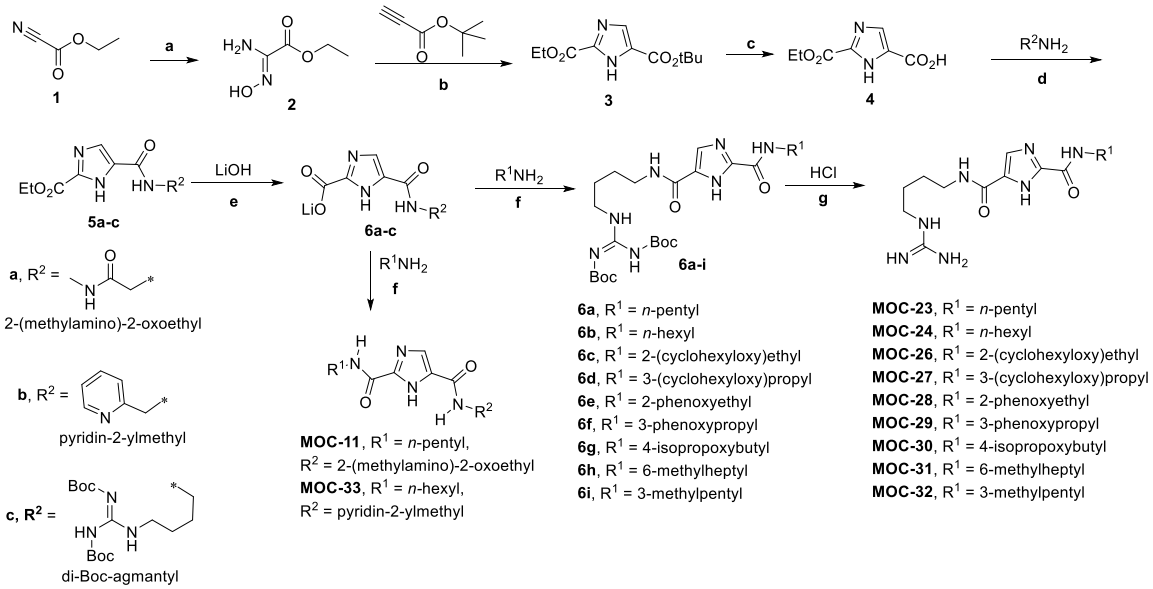

Scheme 1. Synthesis of NS4A peptidomimetics and structure of screened compounds. Reagents and conditions: (a) $NH_2OH{\cdot}HCl$, Na_2CO_3, EtOH, H_2O (b) Et_3N, toluene, MW (120 °C, 300 W, 13 min. (c) TFA, dichloromethane (DCM), 12 h. (d) EDCI, HOBt, DIPEA, THF, room temperature to 60 °C (e) THF, H_2O (f) T3P, THF, 24-48 h. (g) Dioxane, DCM.

2.4. Comparative Binding Evaluation of MOC Compounds Using Differential Static Light Scattering (DSLS)

We studied the binding of MOC compounds with NS3 by differential static light scattering (DSLS) [40]. The NS3 domain stability upon binding to NS4A was measured by monitoring denatured protein aggregation upon increasing temperature gradually from 25.0 to 85.0 °C (0.5 °C increments) at 600 nm. If a ligand binds to the protein increases a protein's aggregation temperature (T_{agg}) [40,41]. DSLS provides an advantage of being label-free binding assay technique and ΔT_{agg} (Liganded protein-Free protein) can be used to assess relative binding affinities of ligands [42]. For NS3, ΔT_{agg} that occurred upon binding of MOC compounds were measured and compared to that of $NS4A_{21`-33`}$ as a positive control. MOC-11 (ΔT_{agg} 0.82 ± 0.32 °C), MOC-24 (ΔT_{agg} 0.60 ± 0.14 °C) and MOC-23 (ΔT_{agg} 0.32

Preprints (www.preprints.org) | NOT PEER-REVIEWED | Posted: 24 January 2020 doi:10.20944/preprints202001.0279.v1

Peer-reviewed version available at *Biomolecules* **2020**, *10*, 479; doi:10.3390/biom10030479

± 0.29 °C) demonstrated significant affinities towards NS3, albeit weaker than that of NS4A (ΔT_{agg} 1.50 ± 0.34 °C) (Figure 3).

(A)

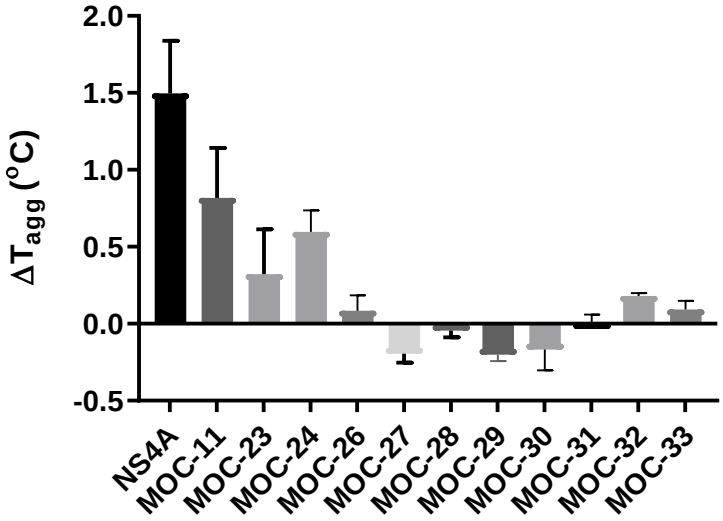

(B)

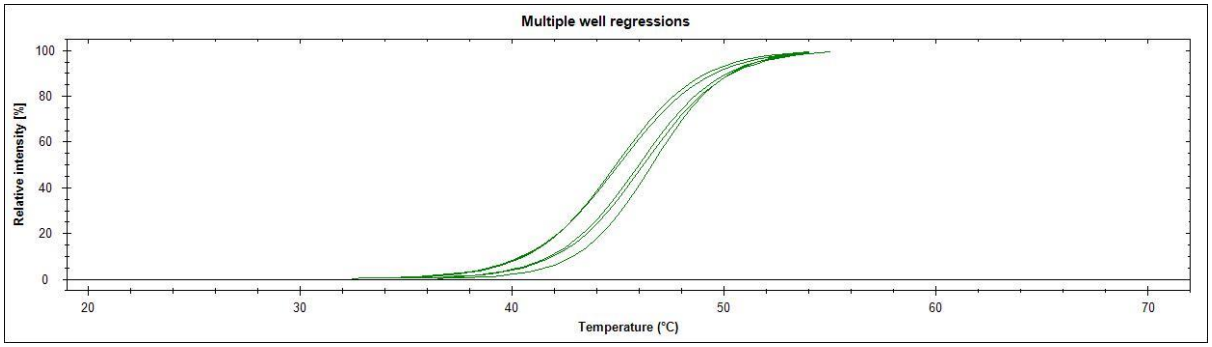

(C)

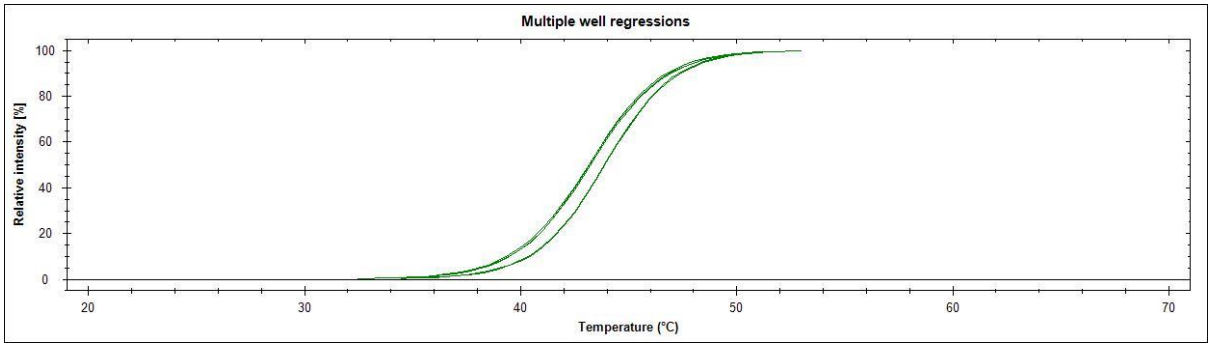

Preprints (www.preprints.org) | NOT PEER-REVIEWED | Posted: 24 January 2020 doi:10.20944/preprints202001.0279.v1

Peer-reviewed version available at Biomolecules 2020, 10, 479; doi:10.3390/biom10030479

(D)

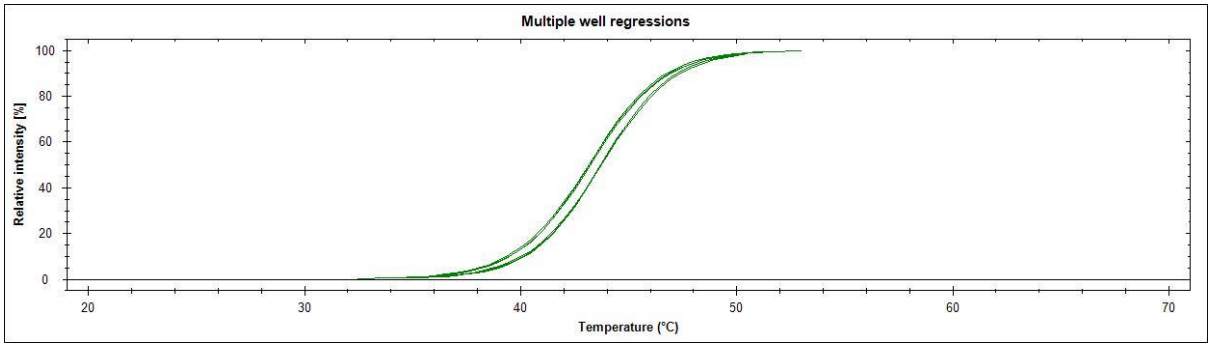

(E)

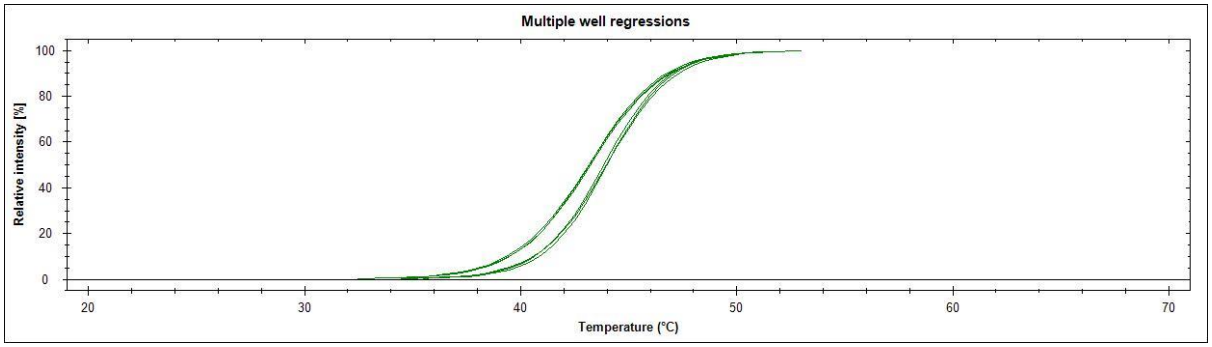

Figure 3. (A) Bar graph representation of changes in thermal stability (ΔT_{agg}) of NS3 when mixed with MOC derivatives or NS4A (n=3). In brief, NS3 domain (15.0 µM) alone (right bundle) or mixed with equimolar equivalent of tested compounds (left bundles): (B) $NS4A_{21`-33`}$, (C) MOC-11, (D) MOC-23 and (E) MOC-24. The final volume was adjusted to 100 µL, the mixture was incubated at room temperature with gentle shaking for 2h. Protein aggregation was monitored on Stargazer-2 by tracking the change in scattered light by taking snapshot images of the plate every 0.50 °C. The pixel intensities were proportional to degree of aggregation. A proprietary software (Stargazer AIR) was used to calculate the aggregation temperature (T_{agg}) illustrated in (A) as well as generating the plot graphs (B-E).

2.5. Fluorescence Anisotropy (FA) Competition Assay of MOC Compounds with NS4A

This assay measures the potency by which synthetic peptidomimetics affect the binding of labeled $NS4A_{21`-33`}$. Before testing the MOC compounds, the binding affinity of fluorescein isothiocyanate $NS4A_{21`-33`}$ (FITC-$NS4A_{21`-33`}$) was first determined (See Supplementary Material Figure S3) based on our previous work [29]. For this particular protein batch, the

Preprints (www.preprints.org) | NOT PEER-REVIEWED | Posted: 24 January 2020 doi:10.20944/preprints202001.0279.v1

Peer-reviewed version available at Biomolecules 2020, 10, 479; doi:10.3390/biom10030479

optimal ratio to be used in FA affinity test was calculated to be 0.5 M NS3 and 0.1 M FITC-$NS4A_{21`-33`}$. Compounds that efficiently compete with $NS4A_{21`-33`}$ are expected to decrease the fluorescence emitted from NS3/FITC-$4A_{21-34`}$ mixture. Results showed that MOC-24 had the strongest competition potency in this assay because it showed a half maximal inhibitory concentration (IC_{50}) of 1.9 µM (Table 1, Figure 4), followed by MOC-23 (4.7 µM). MOC-32 also showed moderate inhibition of NS4A binding (Competition IC_{50} 7.7 µM). Compounds MOC-11, MOC-30, MOC-31 and MOC-33 demonstrated weaker affinity at competition IC_{50} values between 12 and 40 µM, while MOC-26, MOC-27, MOC-28 and MOC-29 exerted no inhibition of NS4A binding up to 100 µM.

Compound	Competition IC_{50} ± SEM (µM)
MOC-11	17.3 ± 1.22
MOC-23	4.70 ± 0.327
MOC-24	1.91 ± 0.119
MOC-26	>100
MOC-27	>100
MOC-28	>100
MOC-29	>100
MOC-30	28.5 ± 8.55
MOC-31	12.1 ± 1.69
MOC-32	7.74 ± 0.240
MOC-33	40.3 ± 24.0

Table 1. Inhibition of $NS4A_{21`-33`}$ binding with NS3 by MOC compounds and NS3 inhibition. SEM = Standard Error of Mean.

Preprints (www.preprints.org) | NOT PEER-REVIEWED | Posted: 24 January 2020 doi:10.20944/preprints202001.0279.v1

Peer-reviewed version available at Biomolecules 2020, 10, 479; doi:10.3390/biom10030479

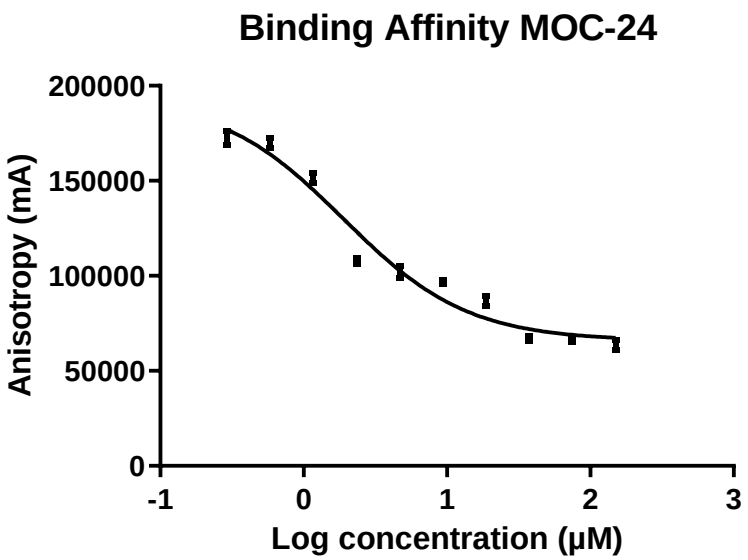

Figure 4: Fluorescence anisotropy competition assay for MOC-24. In brief, FITC-NS4A$_{21`-33`}$ (0.1 µM) was mixed with NS3 (0.5 µM) and variable concentration of MOC-24 (X axis) for 60 minutes. The emitted fluorescence was measured (480/520 nm) proportional to the amount bound FITC-NS4A$_{21`-33`}$ (Y axis).

2.6. Enzyme Inhibition Assay

MOC-24 was selected for a qualitative testing for its inhibition of NS3 protease activity. Experiments were carried out using the SensoLyte® 520 HCV Protease Assay Kit. This assay measures recovered fluorescence emitted upon cleavage of the labelled peptide substrate representing the NS4A/NS4B junction [43]. Considering that NS3 without NS4A is almost a thousand-time less catalytic [23], the method was modified to suit the purpose of our allosteric inhibition assay. For instance, we used a large amount of free NS3 protein (2.00 µM) because smaller concentration did not show measurable catalytic activity in absence of cofactors. Addition of 4.00 µM amounts of MOC-24 resulted in complete loss of NS3 catalytic activity. As a positive control, an equimolar mixture of NS4A with NS3 (equimolar, 2.00 µM each) caused only 9-fold increase in the catalytic activity of the

Preprints (www.preprints.org) | NOT PEER-REVIEWED | Posted: 24 January 2020 doi:10.20944/preprints202001.0279.v1

Peer-reviewed version available at Biomolecules 2020, 10, 479; doi:10.3390/biom10030479

enzyme (Figure 5) which were far less than reported value [23], possibly due to large amount of protein used.

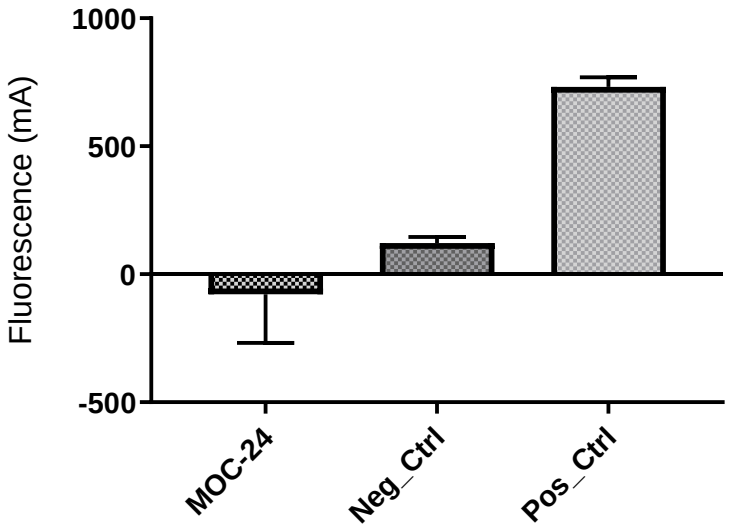

Figure 5. Effect of MOC-24 on the NS3 activity (*n* = 5). In brief, NS3 alone (Neg_Ctrl), or mixed with MOC-24 or NS4A$_{21`-33`}$ (Pos_Ctrl) were mixed with substrate (FRET peptide), derived from the cleavage site of HCV NS4A/NS4B. The emitted fluorescence was proportional to catalytic activity of the enzyme (*n* = 3).

2.7. Molecular Dynamic Simulation for MOC-24 and MOC-26

In order to rationalize the differences in binding affinity of MOC-24 and MOC-26 (as representatives of active and inactive compounds, respectively), we performed molecular dynamics (MD) simulation for 20.0 nano-seconds (ns) at 300 ^{o}K for after manual docking of both compounds to place them to the intended pocket followed by energy relaxation. The MD simulation tries to disrupt non-bonding interactions with of the ligand with the binding site residues by applying energy snapshots that result in conformational excitations followed by relaxations until an equilibration occurs [44]. Equilibration of the system can be determined by plotting protein's backbone-ligand root mean square deviation (PL-RMSD) *vs.* the simulation time. If certain protein-ligand interactions stayed uninterrupted

Preprints (www.preprints.org) | NOT PEER-REVIEWED | Posted: 24 January 2020 doi:10.20944/preprints202001.0279.v1

Peer-reviewed version available at Biomolecules 2020, 10, 479; doi:10.3390/biom10030479

after the equilibrium reached, it indicates higher possibility of occurrence of the postulated binding mode [45].

First, an MD control experiment was performed on NS3/4A$_{21`-32`}$ crystal structure (PDB Code 1NS3). As expected, this viral peptide-protein complex maintained a high degree of stability and low residue fluctuations during most of the simulation period (See Supplementary Material, Figure S4-A). The MD simulation model of MOC-24 demonstrated three important features: a) The ligand resided during all the simulation period (20.0 ns) within the boundaries of presumed binding region of NS4A$_{25`-28`}$ located between the A0 and A1 β-strands; b) The imidazole nucleus had low interaction fluctuations; and c) The *n*-hexyl side chain stayed deep in the hydrophobic pocket accommodating Ile-25` side chain (A video illustration available as part of Supplementary Material). Monitoring the protein-ligand (PL-RMSD) of NS3/MOC-24 simulation indicated that the NS3 protein (backbone atoms) equilibrated its conformational fluctuations after ~10.0 ns and kept the status towards the end of the simulation period (Figure 6). Meanwhile, the ligand (MOC-24) equilibrated at ~ 13.4 ns. Both the protein and the ligand clearly showed the least fluctuations after 17.5 ns until the simulation ended at 20 ns indicating that the complex has reached stability at this binding mode.

Preprints (www.preprints.org) | NOT PEER-REVIEWED | Posted: 24 January 2020 doi:10.20944/preprints202001.0279.v1

Peer-reviewed version available at Biomolecules 2020, 10, 479; doi:10.3390/biom10030479

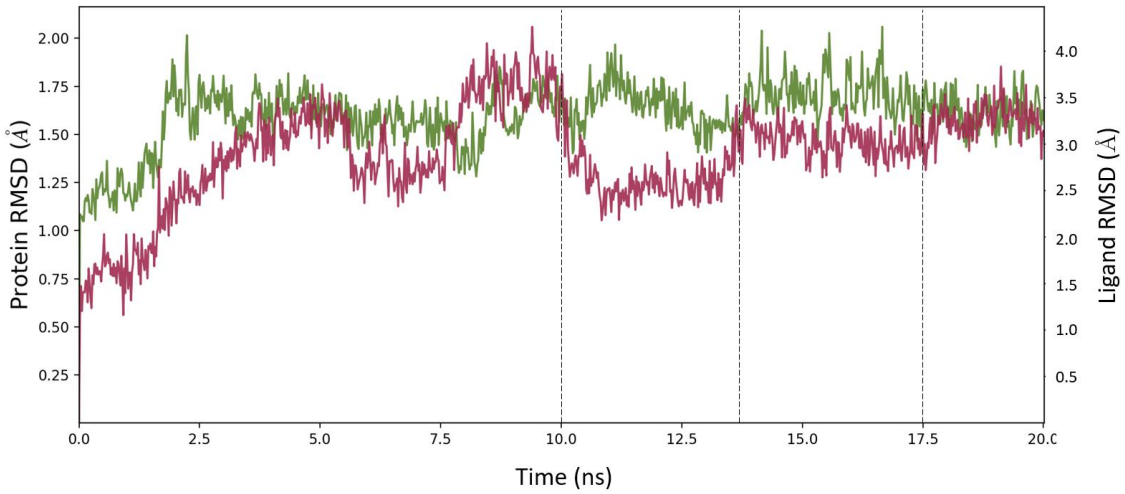

Figure 6. Plot of MOC-24 RMSD (wine-red, right Y scale) and NS3 Protein backbone RMSD (green, left Y scale) against simulation time. The dashed lines are for time points of distinct phases of protein and ligand conformation evolving over simulation time.

Accordingly, we looked carefully at the conformational behavior of the crucial imidazole-2,5-dicarboxamide core at the three phases of the ligand conformational dynamics. The imidazole nucleus, generally, and its NH at position 1, specially, showed low fluctuations (Figure 7). During the first phase (0-10.0 ns), we noticed that the imidazole-2,5-dicarboxamide core kept two hydrogen bonding attractions with A1 β-strand's Val-35, the presumed situation according to the design hypothesis described above (Figure 8A). Around 10 ns, the imidazole ring started to detect and interact with Gln-8, a residue within the opposite A0 β-strand located at the periphery of the NS3 protein (Figure 8B). At ~13.3 ns, the imidazole-2,5-dicarboxamide settled to embrace Gln-8 backbone *via* two hydrogen bonding interactions and, in the process, it lost contacts with Val-35. After this major flip, the imidazole committed to Gln-8 and showed low fluctuations towards the end of the simulation (Figure-8C and 8D).

Preprints (www.preprints.org) | NOT PEER-REVIEWED | Posted: 24 January 2020 doi:10.20944/preprints202001.0279.v1

Peer-reviewed version available at Biomolecules 2020, 10, 479; doi:10.3390/biom10030479

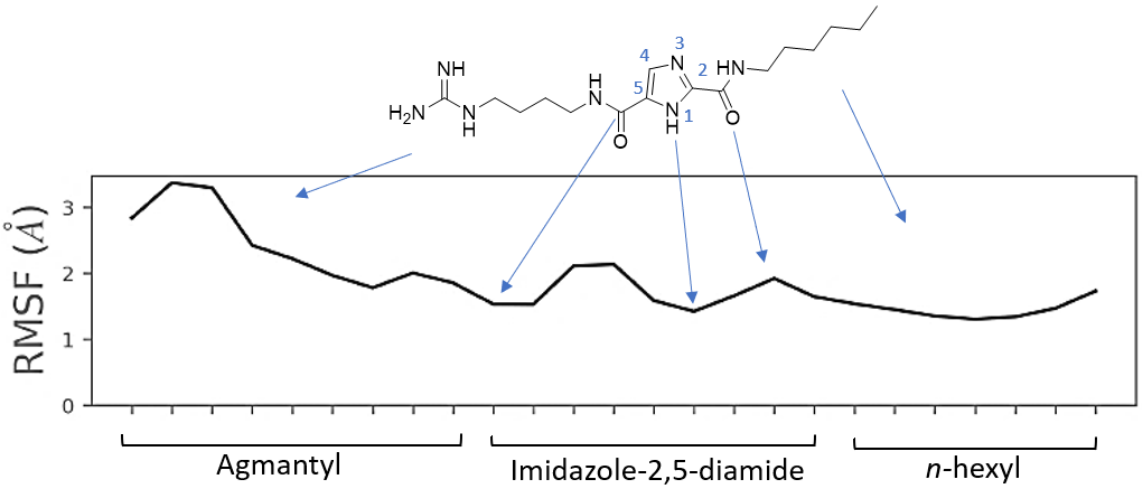

Figure 7. Root mean square fluctuations (RMSF) of MOC-24 heavy atoms. Note highest conformational instability of the guanidine terminal and low motility of both imidazolediamide core the n-hexyl side chain.

A

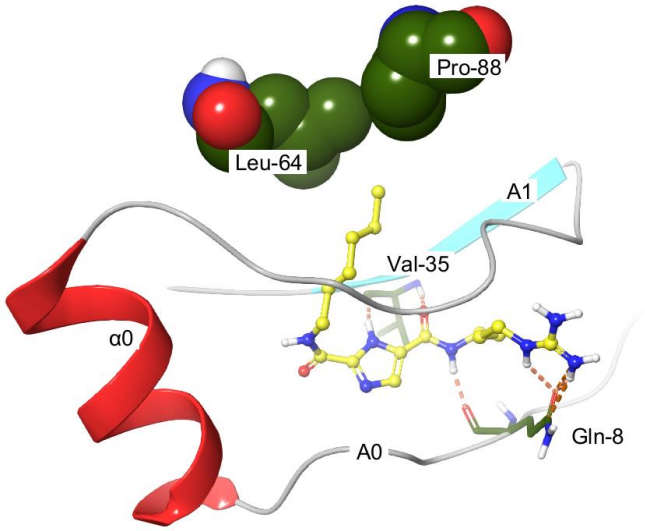

B

Preprints (www.preprints.org) | NOT PEER-REVIEWED | Posted: 24 January 2020 doi:10.20944/preprints202001.0279.v1

Peer-reviewed version available at *Biomolecules* **2020**, *10*, 479; doi:10.3390/biom10030479

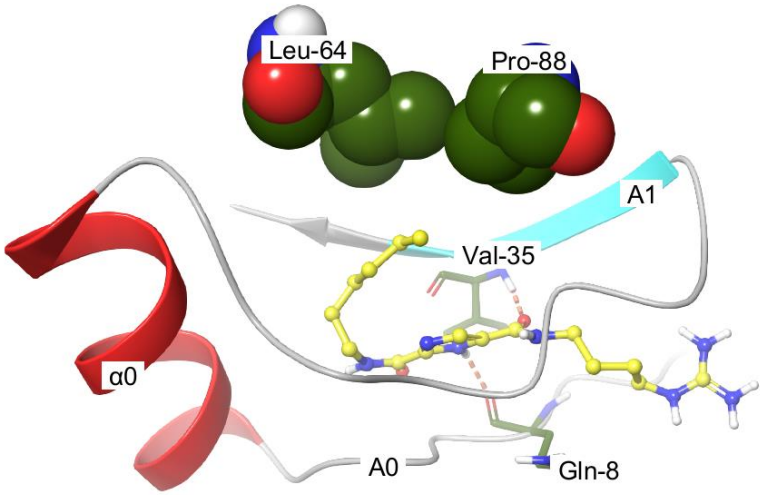

C

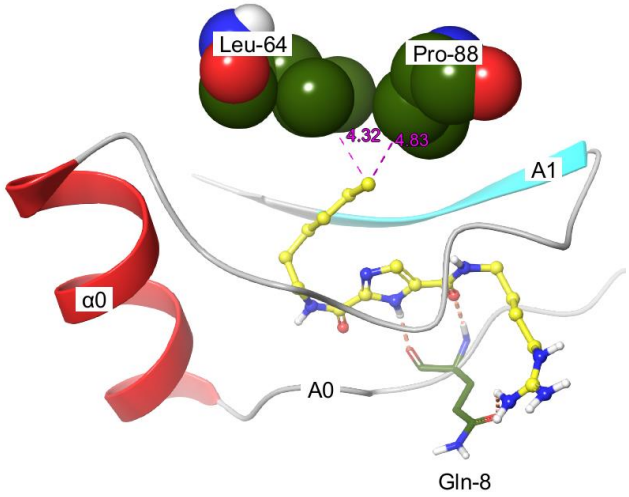

D

Preprints (www.preprints.org) | NOT PEER-REVIEWED | Posted: 24 January 2020 doi:10.20944/preprints202001.0279.v1

Peer-reviewed version available at Biomolecules 2020, 10, 479; doi:10.3390/biom10030479

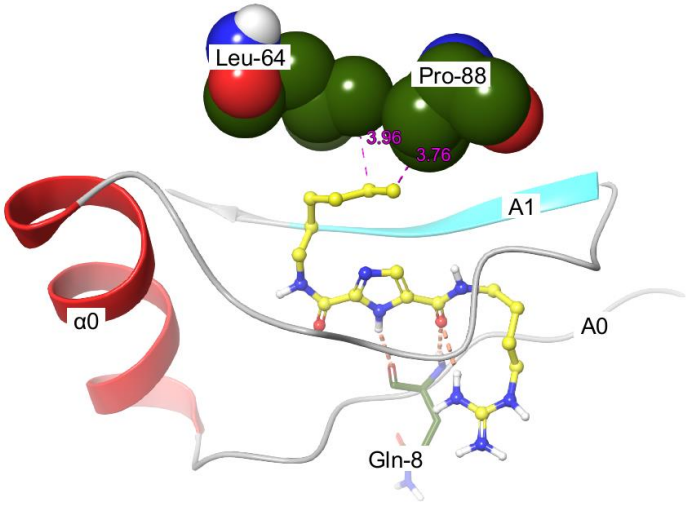

Figure 8. Interactions of MOC-24 (yellow) with the most important residues (green) at the significant time frames. A) At the start of the simulations, B) at 10 ns when protein stability started, C) at 13.4 when imidazole-2,5-diamide completely flipped, and D) at the end of the MD simulation. Hydrogen bonds are dashed lines with orange color and valid VdW interaction distances are displayed in dashed line and numerical values in Angstroms with magenta color.

The behavior of the hydrophobic substituent attached to the C2 carboxamide of MOC-24 was a critical issue in our model because this moiety of the compound is the only difference between the active MOC-24 and the inactive MOC-26. The N^2-(*n*-hexyl) group of MOC-24 stayed in the deep hydrophobic pocket although it did not show strong commitments to a certain amino acid in the active site. In this regard, Leu-64 and Pro-88 were the most interacting residues with the *n*-hexyl side chain. This hydrophobic *n*-hexyl showed low RMSF compared to the other polar N^5-agmantyl substituent (Figure 7). The MD simulation could describe lack of binding of the inactive MOC-26 which contains a bulkier hydrophobic substituent that ends with a cyclohexyl group. As the simulation time progressed, this cyclohexyl group was forced outside the hydrophobic pocket. In fact, the whole MOC-26 molecule left the NS4A binding region located in between A0 and A1 β-sheets. The imidazole made only minor contacts with Gln-8 while most of the ligand clearly popped outside to settle near the protein surface (Figure 9). This movement indicates lack

of affinity of MOC-26 to the NS4A binding pocket. The last point obtained from the MD study was about the role of the polar agmantyl group in MOC-24. This group served as a polar head suitable for the micro environment around the Arg-28` of the bound NS4A. It alternated interactions at the periphery during the simulation between Glu-30, Gln-28 and the solvent. This is not an odd observation because Arg-28` showed similar behavior in reported NS3/4A crystal structures [46-48] (See Supplementary Material, Figure S4-B).

Preprints (www.preprints.org) | NOT PEER-REVIEWED | Posted: 24 January 2020 doi:10.20944/preprints202001.0279.v1

Peer-reviewed version available at Biomolecules 2020, 10, 479; doi:10.3390/biom10030479

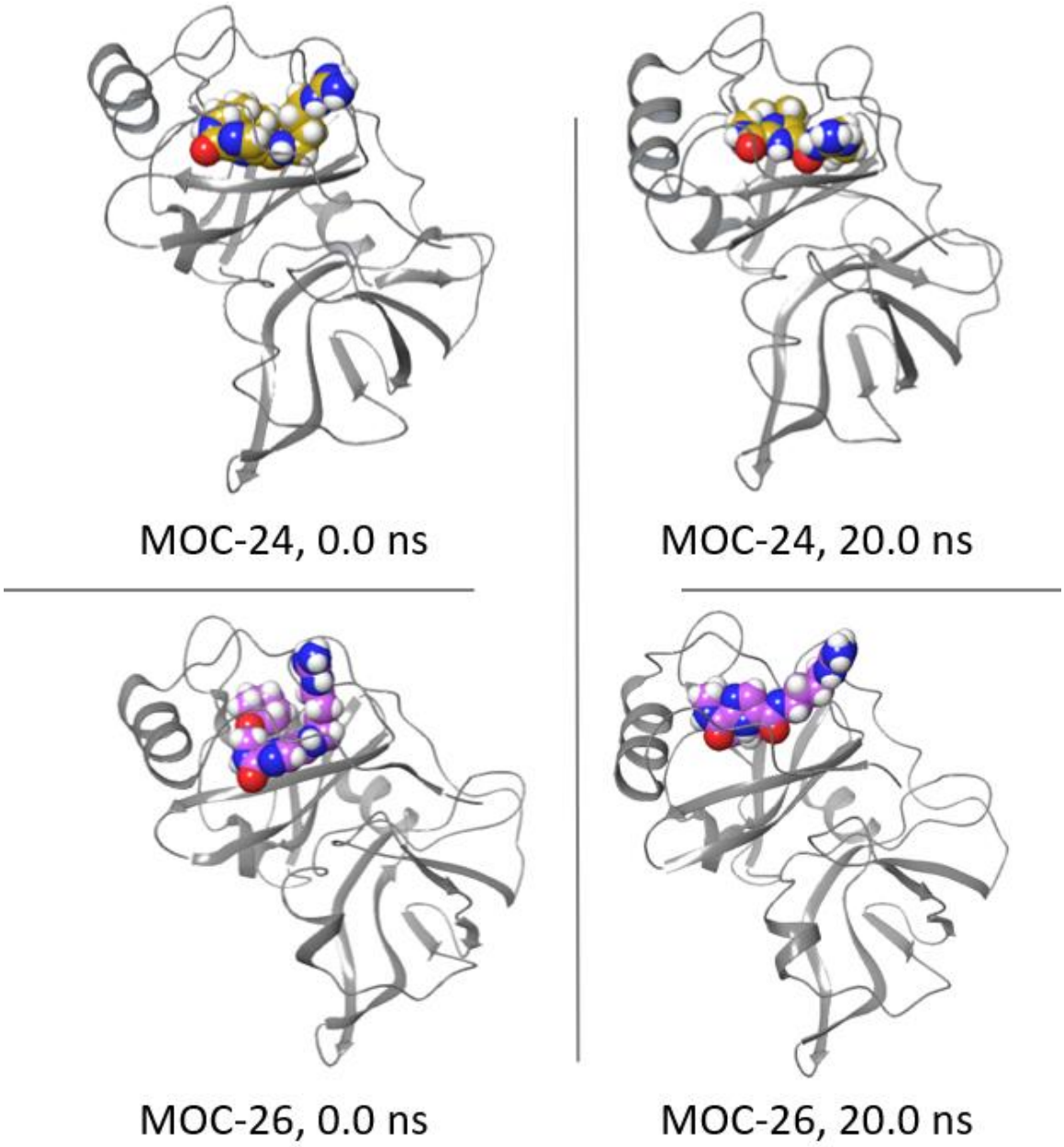

Figure 9. Change in positioning of MOC-24 (upper, ligand colored golden yellow) and MOC-26 (lower, ligand colored magenta). The right images are for PL complexes before the start of MD simulations and the left two images are for PL complexes after completion of the MD simulations.

3. DISCUSSION AND CONCLUSION

The introduction of DAA combinations allowed broadening the efficacies of HCV treatment to the pan-genotypic orbit. These combinations were made possible by identifying more targets in the viral proteome. For instance, Vosevi® is a combination of

sofosbuvir (NS5B inhibitor), velpatasvir (NS5A inhibitor), and voxilaprevir (NS3/4A protease inhibitor) that covers HCV Genotypes 1-6. We were truly motivated to the inclusion of NS4A competitors as a less studied target aiming to further embolden the arsenal of DAA combinations. However, our extensive literature search could not find a precedent of designing and/or screening small molecule peptide mimics of NS4A. An additional advantage of targeting NS4A is that this vital component is a versatile small peptide commonly expressed in all *Flaviviridae* family of viruses which include, besides HCV, other dangerous pathogenic viruses such as Zika, West Nile and Dengue viruses. Therefore, effective NS4A peptidomimetics may constitute a possible general approach to combat *Flaviviridae.*

Our approach of the peptidomimetic design depended on simple observations: The conformation of the bound NS4A and the relevance of the residues involved in the design. The virtually designed 1*H*-imidazole-2,5-dicarboxamide appeared to reproduce satisfactorily the stereochemistry of these NS4A features. Indeed, we could experimentally confirm that such compounds display binding affinity towards the NS3 genotype-4, the most abundant type in the Middle East [49,50]. Our work allowed quantifying the binding affinity of our designed MOC compounds. The FA competition assay confirmed their binding to the NS4A binding site between A0 and A1 β-strands. Both DSLS and FA assays generally agreed that MOC-11, MOC-23 and MOC-24 exerted good affinities towards NS3. Structurally, the three compounds contain *n*-pentyl or its homologue *n*-hexyl at R^1 position. Larger hydrophobic groups at this position (MOC-26 to MOC-31) had lower binding affinities in both DSLS and FA tests indicating that the pocket has limited bulk tolerance. Regarding the R^2 position, all screened compounds contained an agmantyl group, except

for MOC-11 and MOC-33. The Agmantyl group was chosen as a mimicry of the NS4A's Arg-28`. In addition, the agmantyl moiety was hypothesized to act as a hooking group and direct the imidazole scaffold to its intended position. MOC-11 and MOC-33 were synthesized appending two different polar groups at R^2 position. MOC-11 encompassed a glycinyl moiety (backbone mimic). Compared to the agmantyl analogue MOC-23, MOC-11 produced a higher increase in T_{agg}, but showed a lower competition potency in the FA assay. This indicates that the presence of the Arg-28` side chain may be replaced with another polar group. This SAR feature is important for future research towards optimization of the NS4A peptidomimetics by getting rid of the guandinyl moiety, a less desirable group in drug discovery due to high ionizability and poor pharmacokinetics. MOC-33 presented a more radically different variant from the Arg-28` side chain group. This compound showed much weaker binding in both tests, indicating that a successful peptide mimic should include close mimics of those amino acid features (glycinyl or agmantyl).

MOC-24, a homologue of MOC-23, exerted confirmed binding activities as revealed in both DSLS and FA tests. It showed ~1/3 of the thermal stabilization (ΔT_{agg}) of NS3 when compared to the natural cofactor $NS4A_{21`-33`}$. In the FA assay, it demonstrated the highest ability to displace $NS4A_{21`-33`}$ from NS3 binding among the tested compounds. Moreover, our *in vitro* protease assay showed that MOC-24 can inhibit NS3 by forming an inactive complex. However, this test could not be further developed to a quantitative application due to the very week catalytic activity of the NS3 in *in vitro* conditions. The MD simulation, conducted in the course of this study, was useful in validating the design hypothesis and in explaining the binding potency differences between MOC-24 and MOC-26 (as

representatives for active and inactive compounds, respectively). It was remarkable that MOC-24 stayed in the region between A0 and A1 β-sheets and the *n*-hexyl group completely buried deep in a hydrophobic pocket all the MD simulation time. A question that frequently comes to mind is what conformational effects occurred consequently to binding of NS4A peptidomimetics (e.g. MOC-24)? This question should be of secondary importance, anyway, because prevention of NS4A binding by non-peptide mimics should lead to inability of NS3 to do its catalytic function.

Collectively, our work introduces a new strategy to interfere with NS3 protease activity by compounds that represent non-peptide mimics of an NS4A fragment (Ile-25` to Arg-28`). We must acknowledge that our compounds represented only 4 amino acids at the core of NS4A and covered a limited region of the binding site. Considering their promising activities and limited molecular weight (MOC-24, M.Wt. 351.5), imidazole-2,5-carboxamides prove that NS4A binding is a good target for discovery of newer generation of DAAs. Our work can be considered a bridging between peptide and non-peptide mimics of NS4A. Our expandable leads pave the way for future discovery of NS4A competitors as clinical candidates.

4. EXPERIMENTAL

4.1 Chemical Synthesis

Solvents and reagents were purchased from Sigma-Aldrich (USA), VWR (USA) or Alfa Aesar (UK). When needed, solvents were dried according procedures described in literature. Unless stated otherwise, reactions were performed under inert atmosphere of nitrogen. Microwave reactions (MW) were performed using Milestone StartSynth™ reactor (Milestone Inc., Italy). Melting points (Mp) were determined in open capillary

tubes using Electrothermal apparatus (Stuart, UK) and are uncorrected. NMR were recorded on Bruker DPX-300 MHz (Bruker, Switzerland). HPLC-Mass Spectrometry were performed on Agilent 1100 / ZQ MSD including C18 column and diod-array UV detector. The mobile phase (containing 0.01 M ammonium acetate) was gradient starting from 20% acetonitrile/80% water to 80% acetonitrile/20% water. Purities are reported according to percentage of Peak Areas at wavelength 254 nm. According to LC/MS analyses, all compounds in this study were confirmed to have 95% purity or higher. Infrared spectra were recorded on a Thermo Scientific Nicolet iS10 Fourier transform (FT)-IR Spectrometer. In this report, we only listed the important IR stretching bands, including NH, OH, CH, C=O, C=N and/or C=C. In FT-IR, all samples were measured neatly. The synthesis of intermediates 1,2-Bis(*tert*-butoxycarbonyl)-3-(4-aminobutyl)guanidine [39], ethyl (*Z*)-3-amino-3-(hydroxyimino)propanoate (**2**) [38], and 5-(*tert*-butyl) 2-ethyl 1H-imidazole-2,5-dicarboxylate (**3**) [36,37] are described below and their characterization data were found agreeing with literature data.

4.1.1. Synthesis of 5-(tert-butyl) 2-ethyl 1H-imidazole-2,5-dicarboxylate (3)

Water (0.6 mL/mmol) is added dropwise over a period of 2 h to a stirred mixture of ethyl cyanoformate **1** (1.0 equiv., 3 g, 30.3 mmol), hydroxylamine hydrochloride (1.5 equiv., 3.16 g, 45.4 mmol) and sodium carbonate (0.77 equiv., 2.470 g, 23.3 mmol) in ethanol (24.0 mL) at room temperature (rt). Upon completion, the reaction was quenched, and the solvent was removed under vacuum. The resulting residue was extracted with dichloromethane, and the combined organic layers were washed with brine, dried over $MgSO_4$, filtered and concentrated to afford a white solid of the intermediate (*Z*)-2-amino-2-(hydroxyimino) acetate (**2**). The intermediate **2** was recrystallized from chloroform and

n-heptane to afford white crystals (1.881 g, 47%), Mp 59-61 ºC and used without further purification to the next step. This intermediate (1.0 equiv., 1.320 g, 10 mmol) and *tert*-butyl propiolate (1.0 equiv., 1.262 g, 10 mmol) and Et_3N (1.0 equiv., 1.40 mL, 1 mmol) were added to toluene (5.50 mL). The resulting solution was microwave-irradiated at 120 °C for 10 min at 300 W after heating ramp for 3 min. The solvent was evaporated, and the final product was purified by crystallization from ethyl acetate (EtOAc)/hexane to obtain 128 mg (53.3%) of **3**, Mp 160-165 ºC. ^{1}H NMR (300 MHz, DMSO DMSO-d_6) δ_H ppm 13.72 (br., 1 H), 7.87 (s, 1 H), 4.34 (q, J = 7.2 Hz, 2 H), 1.51 (s, 9 H), 1.32 (t, J = 7.0 Hz, 3 H); ^{13}C NMR (75 MHz, $CDCl_3$) δ_c 169.7, 136.5, 129.5, 129.1, 128.9, 127.8, 123.8, 29.7; IR (FT-IR, cm^{-1}): 3025.3, 2916.8, 2843.6, 1695.0, 1619.3, 1594.0, 1571.3, 1505.7; LC-MS (ESI), RT = 1.41 min, *m/z* 241.3 $[M + H]^+$

4.1.2. Synthesis of 2-(ethoxycarbonyl)-1H-imidazole-4-carboxylic acid (4)

A solution of 5-*tert*-butyl 2-ethyl 1H-imidazole-2,5-dicarboxylate (1 equiv., 4.29 g, 17.6 mmol) and TFA (21.1 mL) in DCM (14.0 mL) was stirred for 12h at rt. The solvent was evaporated under vacuum and the remaining residue was treated with MeOH (70.0 mL) and filtered to give **4** as a yellow solid (2.841 g, 86.29%), Mp >230 ºC (decomposed). ^{1}H NMR (300 MHz, DMSO- DMSO-d_6) δ_H ppm13.72 (br. s, 1 H); 12.59 (br. s, 1 H), 7.91 (s, 1H), 4.33 (q, J = 6.9 Hz, 2H), 1.32 (t, J = 7.0 Hz, 3H); LC-MS (ESI), RT = 1.55 min, *m/z* 185.3 $[M + H]^+$.

4.1.3. General procedure for the synthesis of ethyl 4-(N-substituted carbamoyl)-1H-imidazole-2-carboxylate (5a-5c)

Under inert atmosphere, the carboxylic acid (1.0 equiv., 5.21 mmol) was dissolved in dry THF (26 mL) then EDCI (1.0 equiv., 0.998 g, 5.21 mmol), HOBt (1.0 equiv., 0.704 mg,

5.21 mmol), diisopropyl ethylamine (DIPEA) (1.5 equiv., 1.35 mL, 7.80 mmol) and the amine R^2NH_2 (1.2 equiv., 6.25 mmol) were added orderly. The mixture was stirred at rt for 1h then heated to 60°C. After 3h, EDCI (0.5 equiv., 0.500 g, 2.60 mmol), HOBt (0.5 equiv., 0.352 g, 2.60 mmol), DIPEA (0.75 equiv., 0.677 mL, 3.90 mmol) were added to the mixture. After completion, the mixture was purified by column chromatography using gradient elution (50-100% EtOAc in cyclohexane).

Ethyl 4-((2-(methylamino)-2-oxoethyl)carbamoyl)-1H-imidazole-2-carboxylate (5a)

Yield was 77%, Mp 74-76 ºC. ^{1}H NMR (300 MHz, DMSO-d_6) δ_H ppm 8.19 (br. s., 1H), 7.81 (s, 2H), 4.35 (q, J = 7.1 Hz, 2H), 3.81 (d, J = 5.6 Hz, 2H), 2.59 (d, J = 4.5 Hz, 3H), 1.33 (t, J = 7.1 Hz, 3H) ; LC-MS (ESI), RT = 1.57 min, *m/z* 255.3 $[M + H]^+$.

Ethyl 5-((pyridin-2-ylmethyl)carbamoyl)-1H-imidazole-2-carboxylate (5b)

The intermediate **5b** was obtained as an oily substance and its yield was 94%. ^{1}H NMR (300 MHz, DMSO-d_6) δ_H ppm 13.24 (br. s. 1 H), 8.69 (t, J = 5.6 Hz, 1H), 8.51 (d, J = 4.1 Hz, 1H), 8.41 (s, 1H), 7.81 (s, 1H), 7.74 (t, J = 7.0 Hz, 1H), 7.19 - 7.35 (m, 2H), 4.53 (d, J = 6.0 Hz, 2H), 4.34 (q, J = 7.1 Hz, 2H), 1.32 (t, J = 7.0 Hz, 3H); LC-MS (ESI), RT = 1.14 min, *m/z* 275.3 $[M + H]^+$.

Ethyl (E)-4-((4-(2,3-bis(tert-butoxycarbonyl)guanidino)butyl)carbamoyl)-1H-imidazole-2-carboxylate (5c)

To a solution of 1,4-diaminobutane (2.0 equiv., 0.303 g, 3.44 mmol) in THF (2.3 mL) is added a solution of 1,3-bis(*tert*-butoxycarbonyl)-2-methyl-2-thiopseudourea (1.0 equiv., 500 mg, 1.72 mmol) in THF (1.7 mL/mmol) within 0.5 h. The solution is stirred at room temperature for 1h. After completion, the solvent was removed under vacuum and the product is purified by column chromatography on silica gel using a mixture of

DCM/MeOH to give [[(4-aminobutyl)amino](carboxyamino)methylene]carbamic acid di-*tert*-butyl ester (0.250 g, 52.9 %); ^{1}H NMR (300 MHz, $CDCl_3$) δ_H ppm 11.51 (br. s., 1 H), 8.36 (br. s., 1 H), 3.40 - 3.52 (m, 2 H), 2.75 (t, *J* = 6.7 Hz, 2 H), 1.51 - 1.71 (m, 4 H), 1.52 (s, 9 H), 1.51 (s, 9 H); LC-MS (ESI), RT = 2.44 min, *m/z* 331.8 $[M + H]^+$. The produced amine [[(4-aminobutyl)amino](carboxyamino)methylene]carbamic acid di-*tert*-butyl ester was reacted with the carboxylic acid **4** according to the general procedure for amide coupling described above (Section 4.1.3). The intermediate **5c** was collected as an oily substance, yield was 0.097 g, 36.2 %. The compound was used into the next step at the same day without further characterization.

4.1.4. General Procedure for synthesis of 6a-6c

The ethyl esters (1.0 equiv.) was dissolved in THF/Water 4:1 (4mL/mmol) then LiOH (3.0 equiv.) was added. The mixture was stirred at rt until completion. Afterwards, the solvent was evaporated under vacuum. The remaining residues was resuspended in EtOH/Toluene and evaporated. No further purification or characterization was performed, and the salts were used for the next step.

N^5-(2-(Methylamino)-2-oxoethyl)-N^2-(n-pentyl)-1H-imidazole-2,5-dicarboxamide (MOC-11)

Under inert atmosphere the lithium salt of **6a** (180 mg, 0.78 mmol) was dissolved in dry THF (2.3 mL, 3 mL/mmol) then propanephosphonic acid anhydride (1.17 mL of 50% solution in THF, 3.0 equiv.) and the *n*-pentylamine (0.11 mL, 1.2 equiv.) were added. The mixture was stirred at room temperature for 72h. After 48h, additional 1.0 equiv. of T3P was added to the mixture. Upon reaction completion, the solvent was evaporated under vacuum, and the residue was purified on a silica gel column with gradient elution

0-20% MeOH in $CHCl_3$ to give 0.107 g (46.0 %) of **MOC-11** as a white solid, Mp. 87 ºC. ^{1}H NMR (300 MHz, methanol-d_4) δ_H ppm 7.76 (s, 1H), 4.04 (s, 1H), 3.74 (t, J = 6.4 Hz, 2H), 3.38 - 3.51 (m, 1H), 2.78 (s, 2H), 1.80 - 2.00 (m, 2H), 1.53 - 1.80 (m, 2H), 1.20 - 1.53 (m, 3H), 0.86 - 1.07 (m, 3H); ^{13}C NMR (75 MHz, methanol-d_4) δ_C ppm 170.8, 48.5, 48.2, 47.9, 47.6, 47.4, 47.1, 46.8, 41.8, 38.9, 29.0, 28.9, 25.0, 22.1, 13.0; LC-MS (ESI), RT = 1.46 min, m/z 296.4 $[M + H]^+$.

N^2-(n-Hexyl)-N^5-(pyridin-2-ylmethyl)-1H-imidazole-2,5-dicarboxamide (MOC-33).

This compound was prepared according to the procedure described above for preparation of **MOC-11** starting from **6b** and *n*-hexylamine to obtain **MOC-33** as an oily substance. Yield was 33%. ^{1}H NMR (300 MHz, methanol-d_4) δ_H ppm 8.52 (d, J = 4.5 Hz, 1H), 7.70 - 7.93 (m, 2H), 7.45 (d, J = 7.9 Hz, 1H), 7.19 - 7.40 (m, 1H), 4.71 (s, 2H), 3.39 (t, J = 7.0 Hz, 2H), 1.51 - 1.76 (m, 2H), 1.37 (br. s., 6H), 0.93 (t, J = 6.4 Hz, 3H); ^{13}C NMR (75 MHz, methanol-d_4) δ_C ppm 158.6, 157.8, 148.5, 137.5, 122.5, 121.9, 121.6, 48.5, 48.2, 47.9, 47.7, 47.4, 47.1, 46.8, 43.7, 39.0, 31.3, 29.2, 26.3, 22.3; LC-MS (ESI), RT = 2.74 min, *m/z* 330.3 $[M + H]^+$.

N^5-(4-Guanidinobutyl)-N^2-(n-pentyl)-1H-imidazole-2,5-dicarboxamide (MOC-23)

The lithium carboxylate salt of **6c** was reacted with *n*-pentylamine according the procedure described above for preparation of **MOC-11**. The collected intermediate *N^5*-[[4-(2,3-bis(*tert*-butoxycarbonyl)guanidino)butyl]carbamoyl]-*N^2*-(*n*-pentyl)-*1H*-imidazole-2,5-dicarboxamide (**7a**) was subjected to deprotection reaction for removal of Boc groups. Thus, it was dissolved in dry DCM (5 mL/mmol), added hydrochloric acid (in 1,4-dioxane solution (5 mL/mmol) was added and the reaction mixture was stirred at rt for 2 h. After completion the reaction mixture was concentrated and dried under

vacuum and purified using preparative HPLC to furnish **MOC-23** (27.3 %), Mp 106 ºC. ^{1}H NMR (300 MHz, methanol-d_4) δ_H ppm 7.83 (s, 1H), 3.36 - 3.60 (m, 5H), 3.25 (br. s., 3H), 1.69 (br. s., 7H), 1.17 - 1.50 (m, 6H), 0.95 (br. s., 4H); ^{13}C NMR (75 MHz, methanol-d_4) δ_C ppm 48.5, 48.3, 48.0, 47.7, 47.4, 47.1, 46.8, 40.8, 39.3, 28.9, 28.7, 25.9, 22.1, 13.0; LC-MS (ESI), RT = 1.90 min, *m/z* 338.4 $[M + H]^+$.

N^5-(4-Guanidinobutyl)-N^2-(n-hexyl)-1H-imidazole-2,5-dicarboxamide (MOC-24)

This compound was prepared according to the procedure described above for synthesis of **MOC-23**. The product was obtained as yellowish oily substance (37.1%). ^{1}H NMR (300 MHz, methanol-d_4) δ_H ppm 7.81 (br. s., 1H), 3.39 - 3.57 (m, 4H), 3.07 - 3.27 (m, 3H), 1.61 - 1.84 (m, 8H), 1.55 (t, *J* = 7.1 Hz, 1H), 1.18 - 1.48 (m, 9H), 0.93 (br. s., 4H); ^{13}C NMR (75 MHz, methanol-d_4) δ_C ppm 48.5, 48.2, 48.0, 47.7, 47.4, 47.1, 46.8, 40.8, 39.2, 31.3, 26.4, 25.9, 22.3, 13.0; LC-MS (ESI), RT = 1.78 min, *m/z* 352.3 $[M + H]^+$

N^2-(2-(Cyclohexyloxy)ethyl)-N^5-(4-guanidinobutyl)-1H-imidazole-2,5-dicarboxamide (MOC-26)

This compound was prepared according to the procedure described above for synthesis of **MOC-23**. The product was obtained as yellowish oily substance (19.4%). ^{1}H NMR (300 MHz, methanol-d_4) δ_H ppm7.76 (br. s., 1H), 3.50 - 3.75 (m, 7H), 3.44 (br. s., 3H), 3.25 (br. s., 3H), 1.81 - 2.09 (m, 5H), 1.63 - 1.81 (m, 9H), 1.45 - 1.63 (m, 2H), 1.11 - 1.44 (m, 7H); ^{13}C NMR (75 MHz, methanol-d_4) δ_C ppm 77.5, 65.6, 48.5, 48.2, 47.9, 47.6, 47.4, 47.1, 46.8, 40.7, 37.0, 31.9, 25.8, 25.6, 23.7; LC-MS (ESI), RT = 2.46 min, *m/z* 213.2 $[M + H]^+$

N^2-(3-(Cyclohexyloxy)propyl)-N^5-(4-guanidinobutyl)-1H-imidazole-2,5-dicarboxamide (MOC-27)

This compound was prepared according to the procedure described above for synthesis of **MOC-23**. The product was obtained as yellowish oily substance (41.8%). ^{1}H NMR (300 MHz, methanol-d_4) δ_H ppm 7.73 (s, 1H), 3.38 - 3.76 (m, 7H), 3.13 - 3.30 (m, 3H), 1.79 - 2.07 (m, 5H), 1.63 - 1.79 (m, 7H), 1.56 (d, J = 7.5 Hz, 1H), 1.12 - 1.42 (m, 5H); ^{13}C NMR (75 MHz, methanol-d_4) δ_C ppm 77.5, 65.6, 48.5, 48.2, 47.9, 47.6, 47.4, 47.1, 46.8, 40.7, 37.0, 31.9, 25.8, 25.6, 23.7; LC-MS (ESI), RT = 1.98 min, *m/z* 408.3 $[M + H]^+$

N^5-(4-Guanidinobutyl)-N^2-(2-phenoxyethyl)-1H-imidazole-2,5-dicarboxamide (MOC-28)

This compound was prepared according to the procedure described above for synthesis of **MOC-23**. The product was obtained as an off-white solid; Mp 137-9 ºC (47.8%). ^{1}H NMR (300 MHz, methanol-d_4) δ_H ppm 8.01 (s, 1H), 7.28 (t, J = 7.9 Hz, 2H), 6.82 - 7.10 (m, 3H), 4.19 (t, J = 5.1 Hz, 2H), 3.84 (t, J = 5.1 Hz, 2H), 3.44 (br. s., 2H), 3.25 (br. s., 2H), 1.69 (br. s., 5H); ^{13}C NMR (75 MHz, methanol-d_4) δ_C ppm 129.2, 114.2, 48.5, 48.2, 47.9, 47.6, 47.4, 47.1, 46.8; LC-MS (ESI), RT = 1.86 min, *m/z* 388.4 $[M + H]^+$

N^5-(4-Guanidinobutyl)-N^2-(3-phenoxypropyl)-1H-imidazole-2,5-dicarboxamide (MOC-29)

This compound was prepared according to the procedure described above for synthesis of **MOC-23**. The product was obtained as an off-white solid Mp 135-8 ºC (37.1%). ^{1}H NMR (300 MHz, methanol-d_4) δ_H ppm 7.73 (s, 1H), 7.13 - 7.38 (m, 2H), 6.80 - 7.05 (m, 3H), 4.10 (t, J = 5.9 Hz, 2H), 3.61 (t, J = 6.7 Hz, 2H), 3.44 (br. s., 2H), 3.14 - 3.30 (m, 2H), 2.11 (quin, J = 6.3 Hz, 2H), 1.52 - 1.84 (m, 5H); ^{13}C NMR (75 MHz, methanol-d_4) δ_C ppm 129.1, 120.4, 114.2, 65.3, 48.5, 48.2, 47.9, 47.6, 47.4, 47.1, 46.8, 40.8, 37.9, 36.4, 29.0, 26.6, 25.8; LC-MS (ESI), RT = 1.51 min, *m/z* 402.3 $[M + H]^+$

N^5-(4-Guanidinobutyl)-N^2-(4-isopropoxybutyl)-1H-imidazole-2,5-dicarboxamide (MOC-30)

This compound was prepared according to the procedure described above for synthesis of **MOC-23**. The product was obtained as an oily substance (38.4%). ^{1}H NMR (300 MHz, methanol-d_4) δ_H ppm 7.73 (s, 1H), 3.35 - 3.74 (m, 8H), 3.14 - 3.28 (m, 2H), 1.69 (br. s., 9H), 1.16 (d, J = 6.2 Hz, 6H); ^{13}C NMR (75 MHz, methanol-d_4) δ_C ppm 71.5, 67.4, 48.5, 48.2, 47.9, 47.6, 47.4, 47.1, 46.8, 40.8, 38.7, 37.9, 27.1, 26.6, 26.1, 25.8, 21.0; LC-MS (ESI), RT = 2.08 min, *m/z* 382.3 $[M + H]^+$.

N^5-(4-Guanidinobutyl)-N^2-(6-methylheptyl)-1H-imidazole-2,5-dicarboxamide (MOC-31)

This compound was prepared according to the procedure described above for synthesis of **MOC-23**. The product was obtained as solid, Mp 83-4 ºC (23.7%). ^{1}H NMR (300 MHz, methanol-d_4) δ_H ppm 7.74 (s, 1H), 3.38 - 3.57 (m, 2H), 3.14 - 3.30 (m, 2H), 1.54 - 1.83 (m, 6H), 1.22 - 1.54 (m, 9H), 0.81 - 1.09 (m, 7H); ^{13}C NMR (75 MHz, methanol-d_4) δ_C ppm 48.5, 48.2, 47.9, 47.6, 47.3, 47.1, 46.8, 40.8, 39.5, 30.6, 28.6, 26.7, 25.8, 23.8, 22.7, 13.0, 9.8; LC-MS (ESI), RT = 1.19 min, *m/z* 380.3 $[M + H]^+$

N^5-(4-guanidinobutyl)-N^2-(3-methylpentyl)-1H-imidazole-2,5-dicarboxamide (MOC-32)

This compound was prepared according to the procedure described above for synthesis of **MOC-23**. The product was obtained as an off-white oily substance (41.2%). ^{1}H NMR (300 MHz, methanol-d_4) δ_H ppm 7.73 (s, 1H), 3.35 - 3.58 (m, 4H), 3.14 - 3.30 (m, 2H), 1.69 (br. s., 6H), 1.35 - 1.59 (m, 3H), 1.24 (td, J = 7.0, 13.7 Hz, 1H), 0.77 - 1.09 (m, 6H); ^{13}C NMR (75 MHz, methanol-d_4) δ_C ppm 48.5, 48.2, 47.9, 47.6, 47.4, 47.1, 46.8, 40.8, 37.1, 35.9, 32.1, 29.1, 26.6, 25.8, 18.0, 10.2; LC-MS (ESI), RT = 1.79 min, *m/z* 352.3 $[M + H]^+$

4.2. Biological Screening

All reagents used in the biological screenings were purchased from Sigma-Aldrich (UK) in molecular biology grade unless stated otherwise.

Preprints (www.preprints.org) | NOT PEER-REVIEWED | Posted: 24 January 2020 doi:10.20944/preprints202001.0279.v1

Peer-reviewed version available at Biomolecules 2020, 10, 479; doi:10.3390/biom10030479

4.2.1. NS3 Protein

4.2.1.1. NS3 constructs

A synthetic gene coding for the HCV NS3 domain of genotype 4a, the most abundant HCV in Saudi Arabia and Egypt [51], was synthesized by GenScript (Hong Kong), the nucleotide sequence was optimized for *E. coli* codon usage. The synthetic gene was cloned as *Nde*I-*Bam*HI fragment into the expression vector pET-3a Novagen®. The obtained construct was sequenced to confirm that we have the right clone and the gene is in the correct frame.

4.2.1.2. NS3 protein Information

Accession GU085486.1

HCV genotype 4a (The most common genotype in Saudi Arabia)[52]

NS3 from 4 to 182 aa (L/E, F/E, I/Q, V/E, L/Q, C/S)

NS4A 632 to 685 aa (i/n)

G svvivgrvnl sgdtayaqqt rgeestqets qtgrdtnenc gevqvlstat qsflgtavng vmwtvyhgag sktisgpkgp vnqmytnvdq dlvgwpsppg vksltpctcg asdlylvtrh advvpvrrrg dtrgallspr pistlkgssg gpllcpmgha aglfraavst rgvakavdfv pveslett mrsp

NS4A/NS3 Fusion protein expression in pET-28a

NS3 protease domain 1-181 aa + N-terminal T7 tag and C-terminal His tag

M ASMTGGQQMG apitayaqqt rglfstivts ltgrdtnenc gevqvlstat qsflgtavng vmwtvyhgag sktisgpkgp vnqmytnvdq dlvgwpsppg vksltpctcg asdlylvtrh advvpvrrrg dtrgallspr pistlkgssg gpllcpmgha aglfraavct rgvakavdfv pveslettmr sGSHHHHHH

Expression in pET-3a

2.3.1.4. Protein expression

The sequence of NS3 domain for genotype 4A, was expressed in *E. coli* Rosette (DE3) pLysS according to standard protocol[14]. Therefore, a synthetic gene for NS3 domain was subcloned in the expression vector pET-3a. In the process, a 100 mL of bacterial culture in Luria Broth medium grew overnight at 37°C and used for inoculation of 10 L LB in a 14-liter fermenter flask (New Brunswick Scientific Co., CT, USA). The media was supplemented with ampicillin 50 µg/mL. The culture grew until the OD_{600} reached 0.5-0.6, then it was cooled to 25°C and 1mM IPTG was added. Expression was followed overnight, and then cells were harvested.

2.3.1.5. Protein purification

The produced protein was purified using equilibrated Ni-NTA beads and the poly-histidine tag was not removed. In the process, cells were re-suspended (1.00 g/5mL) in buffer (50mM HEPES, 0.300 M NaCl, 10.0 % glycerol, 2.00 mM β-mercaptoethanol, pH 8.0). Lysozymes were added (1.00 mg/mL) followed by protease inhibitor cocktail tablet and the suspension was sonicated. Cell lysate was centrifuged to collect the clear supernatant that contained the desired NS3 protein. The protein was purified using pre-equilibrated Ni-NTA beads (Qiagen, USA). Beads were washed with buffer (50.0 mM HEPES, 0.300 M NaCl, 10.0 % glycerol, 2.00 mM β-mercaptoethanol, 20.0 mM imidazole, pH 8.0) and eluted with another buffer (50.0 mM HEPES, 0.300 M NaCl, 10.0 % glycerol, 2.00 mM β-mercaptoethanol, 350 mM imidazole, pH 8.0). Fractions were collected and concentrated using Amicon Ultra-4 3000 MWCO centrifugal device (Millipore, Germany). Protein purity after Ni-affinity purification step was not less than 70.0 %. The purity, as estimated by SDS-PAGE, was sufficient to perform all investigations of this study and the protein

was stable for several hours at test conditions [51]. The concentration of NS3 in the final concentrate was measured using Nanodrop™ nanoscale spectrophotometer.

When needed, further purification of the protein was accomplished on Superdex 75 16/90 column (GE Healthcare, USA) equilibrated in 20.0 mM HEPES, 10 mM DDT, 200 mM NaCl, pH 7.60 run at rate of 1 mL/min followed by SDS-PAGE for purity estimation.

4.2.1. NS4A

The cofactor NS4A and the fluorescent fluorescein isothiocyanate NS4A (FITC-NS4A) were purchased from GenScript (Hong Kong). NS4A structure was identical to that of HCV genotype 4a with two lysine residues added at both the N- and C-termini. Thus, the structure of NS4A used in this study was LL-G_{21}SVVIVGRIVLSG_{33}-LL.

We studied the binding of NS4A and its mutants with NS3 by DSLS using Stargazer-2™ (Harbinger Biotechnology and Engineering Corporation, Toronto, Canada). This method assesses protein stability by monitoring aggregate formation at controlled gradually elevated temperatures [40]. NS3 domain stability upon binding to NS4A was measured by monitoring denatured protein aggregation upon increasing temperature from 25.0 to 85.0 °C (0.5 °C increments) at 600 nm. The T_{agg} values were calculated automatically from raw data using Stargazer-AIR® software. All experiments was repeated three times but using the same batch of NS3 protein.

4.2.3. DSLS Binding Test

NS3 domain (15.0 µM) alone or mixed with equimolar equivalent of tested MOC derivative was added to a binding buffer (20.0 mM HEPES, 10.0 mM DTT, 200 mM NaCl, pH 7.60) to final volume 100 µL. The mixture was incubated at room temperature with gentle shaking for 2h. Afterwards, 10 µL of the mixture was transferred into a clear

bottomed Nunc 384-well plate and covered by 10 µL paraffin oil to minimize evaporation. Protein aggregation was monitored by tracking the change in scattered light that was detected by a Charged Coupled Device (CCD) camera. Snapshot images of the plate were taken every 0.5 °C. The pixel intensities in a preselected region of each well were integrated using image analysis software to generate a value representative of the total amount of scattered light in that region. These intensities were then plotted against temperature for each sample well and fitted to obtain the aggregation temperature (T_{agg}). Aggregation was monitored and analyzed to assess the effect of NS4A and its synthetic analogues on the stability of the NS3 as an indicator of binding. Each experiment was repeated 3 times. Statistical analysis was performed using GraphPad Prism v. 8.0® and Instat® software.

4.2.3. Binding and Competition Assay by Fluorescence Anisotropy

In a 96-well plate, place binding buffer (20 mM HEPES, 10 mM DTT, 200 mM NaCl, pH 7.60), A mixture of NS3 (0.40 µM) and FITC-NS4A (0.10 µM) at the calculated affinity constant concentration. A serial dilution of MOC compounds (dissolved in 1.50% DMSO in binding buffer) (1/2 dilution starting from 150 µM to 0.292 µM) and mixed gently for 60 minutes in a dark place and fluorescence were measured at excitation/emission wavelengths of 480/520 nm. The competition IC_{50} was calculated according to the recommended equation embedded in GraphPad Prism v. 8.0® and Instat® software.

4.2.4. Enzyme inhibition assay

The assay was performed using SensoLyte-520® HCV protease assay kit fluorometric* (Anaspec, Fremont, CA, USA) according to a modified procedure to suite the purpose of determination of allosteric inhibition. NS3 (2.00 µM) was mixed with MOC-24 (4.00 µM) for 15.0 min. Afterwards, 5-FAM/QXL™520 fluorescence resonance energy transfer

(FRET) peptide was added as instructed by the assay kit manual. The sequence of this FRET peptide (5-FAM-SLGRKIQIQ) is derived from the cleavage site of NS4A/NS4B. In the FRET peptide, the fluorescence of 5-FAM is quenched by QXL™520. Upon cleavage into two separate fragments by HCV NS3/4A protease, the fluorescence of 5-FAM is recovered, and can be monitored at 490 nm/520 nm (excitation/emission). Controls included buffer, compound, compound+NS3, NS3+NS4A and FRET peptide separately. All test wells and controls were repeated in triplicates at the same 96-well plate.

4.3. Molecular Modeling

4.3.1. Hardware and Software

The molecular modeling was performed on HP OMEN-X PC (Processor: Intel® Core™ i9-7920x CPU @ 2.9 GHz, Installed Memory (RAM): 32.0 GHz, Operating Systems: Windows 10 Enterprise and Enterprise Linux 7 (Distribution CentOS-7). The molecular computational works were performed using Schrödinger Maestro™ Suite (Schrödinger, New York, USA).

4.3.2. Protein and Ligand Preparation

NS3/4A (non-fusion protein) crystal structure (PDB Code: 1NS3) was downloaded from protein data bank website (rcsb.org). Protein was prepared according to standard procedure in Protein Preparation module of Maestro [53]. Briefly, the first stage included Preprocess followed by simplification of the protein to a monomer, removal of unused ligands and water. Finally an energy minimization was performed using OPLS3e force field [54]. MOC compounds were sketched using ACD/ChemSketch freeware (Advanced Chemistry Development, Inc., Toronto, Canada), saved as sdf file and imported to Maestro. Ligands were optimized using LigPrep standard procedure embedded in the Maestro suite. The

ligands selected for molecular dynamics were merged (by 3D visual guidance) onto prepared NS3 protein after the removal of the co-crystallized $NS4A_{21`-32`}$ peptide to form the complexes that entered the next step.

4.3.3. Molecular Dynamics

Using Desmond's System Builder module, the protein–ligand complex was prepared for the MD simulation by applying OPLS3e molecular mechanics force field after solvation in a water box (Shape, Orthorhombic; Size calculation method, Buffer; Distance from protein, 10 x 10 x 10 Å; Box volume, Minimize volume) that contain 0.15 M NaCl as added ions. Other parameters were used as default in the System Builder.

The resulted solvated ligand-protein complex was subjected to Desmond Molecular Dynamics simulation after setting the following parameters: Simulation time, 20 ns; Recording internal: Trajectory, 10 ps; Approximate number of frames, 1000; Ensemble class, Normal Pressure and Temperature (NPT); Temperature, 300 ^{o}K, Pressure, 1.013 bar. Before starting the MD job, the system was allowed to relax using the default Relaxation Protocol. Other parameters were used as default in the Desmond's Molecular Dynamics.

5. PATENTS

El-Araby, M. E.; Omar, A. M.; El-Faky, M. A.; Soror, S. H.; Khayat, M. T.; Asfour, H. Z.; Bamane, F. H. Imidazole-based Compounds as hepatitis C virus inhibitors, US Application 16/384,472, April 16, 2019.

6. ACKNOWLEDGEMENT

This project was funded by the National Plan for Science, Technology and Innovation (MAARIFAH), King Abdulaziz City for Science and Technology, the Kingdom of Saudi Arabia; Award number 12-BIO3193-03. The authors also, acknowledge with thanks

Science and Technology Unit, King Abdulaziz University for technical support. The research reported in this publication was also supported by funding from King Abdullah University of Science and Technology (KAUST).

7. REFERENCES

1. WHO. Global hepatitis report 2017. Availabe online: https://www.who.int/hepatitis/publications/global-hepatitis-report2017/en/ (accessed on Jan 21, 2020).
2. Friedrich, M.J. Third millennium challenge: hepatitis C. *JAMA* **1999**, *282*, 221-222.
3. Dickson, R.C. Clinical manifestations of hepatitis C. *Clin. Liver Dis.* **1997**, *1*, 569-585.
4. Stanaway, J.D.; Flaxman, A.D.; Naghavi, M.; Fitzmaurice, C.; Vos, T.; Abubakar, I.; Abu-Raddad, L.J.; Assadi, R.; Bhala, N.; Cowie, B., et al. The global burden of viral hepatitis from 1990 to 2013: findings from the Global Burden of Disease Study 2013. *Lancet* **2016**, *388*, 1081-1088, doi:10.1016/s0140-6736(16)30579-7.
5. North, C.S.; Hong, B.A.; Adewuyi, S.A.; Pollio, D.E.; Jain, M.K.; Devereaux, R.; Quartey, N.A.; Ashitey, S.; Lee, W.M.; Lisker-Melman, M. Hepatitis C treatment and SVR: the gap between clinical trials and real-world treatment aspirations. *Gen. Hosp. Psychiatry* **2013**, *35*, 122-128, doi:10.1016/j.genhosppsych.2012.11.002.
6. Panel, A.-I.H.G. Hepatitis C Guidance 2018 Update: AASLD-IDSA Recommendations for Testing, Managing, and Treating Hepatitis C Virus Infection. *Clin. Infect. Dis.* **2018**, *67*, 1477-1492, doi:10.1093/cid/ciy585.
7. Chahine, E.B.; Kelley, D.; Childs-Kean, L.M. Sofosbuvir/Velpatasvir/Voxilaprevir: A Pan-Genotypic Direct-Acting Antiviral Combination for Hepatitis C. *Ann. Pharmacother.* **2018**, *52*, 352-363, doi:10.1177/1060028017741508.
8. Chhatwal, J.; Chen, Q.; Aggarwal, R. Estimation of Hepatitis C Disease Burden and Budget Impact of Treatment Using Health Economic Modeling. *Infect. Dis. Clin. North Am.* **2018**, *32*, 461-480, doi:10.1016/j.idc.2018.02.008.
9. Cuypers, L.; Libin, P.; Schrooten, Y.; Theys, K.; Di Maio, V.C.; Cento, V.; Lunar, M.M.; Nevens, F.; Poljak, M.; Ceccherini-Silberstein, F. Exploring resistance pathways for first-generation NS3/4A protease inhibitors boceprevir and telaprevir using Bayesian network learning. *Infect. Genet. Evol.* **2017**, *53*, 15-23.
10. Li, D.K.; Chung, R.T. Overview of Direct-Acting Antiviral Drugs and Drug Resistance of Hepatitis C Virus. *Methods Mol. Biol.* **2019**, *1911*, 3-32, doi:10.1007/978-1-4939-8976-8_1.
11. Hellard, M.E.; Chou, R.; Easterbrook, P. WHO guidelines on testing for hepatitis B and C–meeting targets for testing. BioMed Central: 2017.
12. Bartenschlager, R.; Baumert, T.F.; Bukh, J.; Houghton, M.; Lemon, S.M.; Lindenbach, B.D.; Lohmann, V.; Moradpour, D.; Pietschmann, T.; Rice, C.M., et al. Critical challenges and emerging opportunities in hepatitis C virus research in

an era of potent antiviral therapy: Considerations for scientists and funding agencies. *Virus Res.* **2018**, *248*, 53-62, doi:10.1016/j.virusres.2018.02.016.

13. Murray, C.L.; Jones, C.T.; Rice, C.M. Architects of assembly: roles of Flaviviridae non-structural proteins in virion morphogenesis. *Nature reviews microbiology* **2008**, *6*, nrmicro1928.
14. Kim, J.L.; Morgenstern, K.A.; Lin, C.; Fox, T.; Dwyer, M.D.; Landro, J.A.; Chambers, S.P.; Markland, W.; Lepre, C.A.; O'malley, E.T. Crystal structure of the hepatitis C virus NS3 protease domain complexed with a synthetic NS4A cofactor peptide. *Cell* **1996**, *87*, 343-355.
15. Kim, D.W.; Gwack, Y.; Han, J.H.; Choe, J. C-terminal domain of the hepatitis C virus NS3 protein contains an RNA helicase activity. *Biochem. Biophys. Res. Commun.* **1995**, *215*, 160-166.
16. Failla, C.; Tomei, L.; De Francesco, R. Both NS3 and NS4A are required for proteolytic processing of hepatitis C virus nonstructural proteins. *J. Virol.* **1994**, *68*, 3753-3760.
17. Lin, C.; Pragai, B.M.; Grakoui, A.; Xu, J.; Rice, C.M. Hepatitis C virus NS3 serine proteinase: trans-cleavage requirements and processing kinetics. *J. Virol.* **1994**, *68*, 8147-8157.
18. Morikawa, K.; Lange, C.M.; Gouttenoire, J.; Meylan, E.; Brass, V.; Penin, F.; Moradpour, D. Nonstructural protein 3-4A: the Swiss army knife of hepatitis C virus. *J. Viral Hepatitis* **2011**, *18*, 305-315, doi:10.1111/j.1365-2893.2011.01451.x.
19. Li, K.; Foy, E.; Ferreon, J.C.; Nakamura, M.; Ferreon, A.C.; Ikeda, M.; Ray, S.C.; Gale, M.; Lemon, S.M. Immune evasion by hepatitis C virus NS3/4A protease-mediated cleavage of the Toll-like receptor 3 adaptor protein TRIF. *Proceedings of the National Academy of Sciences* **2005**, *102*, 2992-2997.
20. Meylan, E.; Curran, J.; Hofmann, K.; Moradpour, D.; Binder, M.; Bartenschlager, R.; Tschopp, J. Cardif is an adaptor protein in the RIG-I antiviral pathway and is targeted by hepatitis C virus. *Nature* **2005**, *437*, 1167-1172.
21. de Wispelaere, M.; Du, G.; Donovan, K.A.; Zhang, T.; Eleuteri, N.A.; Yuan, J.C.; Kalabathula, J.; Nowak, R.P.; Fischer, E.S.; Gray, N.S., et al. Small molecule degraders of the hepatitis C virus protease reduce susceptibility to resistance mutations. *Nature Communications* **2019**, *10*, 3468, doi:10.1038/s41467-019-11429-w.
22. El-Araby, M.E.; Omar, A.M.; El-Faky, M.A.; Soror, S.H.; Khayat, M.T.; Asfour, H.Z.; Bamane, F. Imidazole derivatives as HCV NS3/4A protease inhibitors. 2019.
23. Yan, Y.; Li, Y.; Munshi, S.; Sardana, V.; Cole, J.L.; Sardana, M.; Steinkuehler, C.; Tomei, L.; De Francesco, R.; Kuo, L.C., et al. Complex of NS3 protease and NS4A peptide of BK strain hepatitis C virus: a 2.2 Å resolution structure in a hexagonal crystal form. *Protein Sci.* **1998**, *7*, 837-847, doi:10.1002/pro.5560070402.
24. Lin, C.; Thomson, J.A.; Rice, C.M. A central region in the hepatitis C virus NS4A protein allows formation of an active NS3-NS4A serine proteinase complex in vivo and in vitro. *J. Virol.* **1995**, *69*, 4373-4380.
25. Butkiewicz, N.J.; Wendel, M.; Zhang, R.; Jubin, R.; Pichardo, J.; Smith, E.B.; Hart, A.M.; Ingram, R.; Durkin, J.; Mui, P.W., et al. Enhancement of hepatitis C virus NS3 proteinase activity by association with NS4A-specific synthetic peptides:

identification of sequence and critical residues of NS4A for the cofactor activity. *Virology* **1996**, *225*, 328-338, doi:10.1006/viro.1996.0607.

26. Shimizu, Y.; Yamaji, K.; Masuho, Y.; Yokota, T.; Inoue, H.; Sudo, K.; Satoh, S.; Shimotohno, K. Identification of the sequence on NS4A required for enhanced cleavage of the NS5A/5B site by hepatitis C virus NS3 protease. *J. Virol.* **1996**, *70*, 127-132.
27. Tomei, L.; Failla, C.; Vitale, R.L.; Bianchi, E.; De Francesco, R. A central hydrophobic domain of the hepatitis C virus NS4A protein is necessary and sufficient for the activation of the NS3 protease. *J. Gen. Virol.* **1996**, *77*, 1065-1070.
28. El-Araby, M.E.; Omar, A.M.; El-Faky, M.A.; Soror, S.H.; Khayat, M.T.; Asfour, H.Z.; Bamane, F.H. Peptide Inhibitors of HCV NS3/4A Protease Comprising Non-Proteinogenic Amino Residues. April 1, 2019, 2019.
29. El-Araby, M.E.; Omar, A.M.; Soror, S.H.; Arold, S.T.; Khayat, M.T.; Asfour, H.Z.; Bamane, F.; El-Faky, M.A. Synthetic bulky NS4A peptide variants bind to and inhibit HCV NS3 protease. *Journal of Advanced Research* **2020**, https://doi.org/10.1016/j.jare.2020.01.003, doi:https://doi.org/10.1016/j.jare.2020.01.003.
30. Joyce, M.; Williams, M.; Hindsgaul, O.; Tyrrell, D. Inhibitors of hepatitis C virus protease. Sep 18, 2003.
31. De Francesco, R.; Pessi, A.; Steinkühler, C. Mechanisms of hepatitis C virus NS3 proteinase inhibitors. *J. Viral Hepatitis* **1999**, *6*, 23-30.
32. Hamad, H.A.; Thurston, J.; Teague, T.; Ackad, E.; Yousef, M.S. The NS4A cofactor dependent enhancement of HCV NS3 protease activity correlates with a 4D geometrical measure of the catalytic triad region. *PLoS One* **2016**, *11*, e0168002.
33. Jiang, Y.; Andrews, S.W.; Condroski, K.R.; Buckman, B.; Serebryany, V.; Wenglowsky, S.; Kennedy, A.L.; Madduru, M.R.; Wang, B.; Lyon, M., et al. Discovery of danoprevir (ITMN-191/R7227), a highly selective and potent inhibitor of hepatitis C virus (HCV) NS3/4A protease. *J Med Chem* **2014**, *57*, 1753-1769, doi:10.1021/jm400164c.
34. Soumana, D.I.; Kurt Yilmaz, N.; Ali, A.; Prachanronarong, K.L.; Schiffer, C.A. Molecular and Dynamic Mechanism Underlying Drug Resistance in Genotype 3 Hepatitis C NS3/4A Protease. *J Amer Chem Soc* **2016**, *138*, 11850-11859, doi:10.1021/jacs.6b06454.
35. Taylor, J.G.; Zipfel, S.; Ramey, K.; Vivian, R.; Schrier, A.; Karki, K.K.; Katana, A.; Kato, D.; Kobayashi, T.; Martinez, R., et al. Discovery of the pan-genotypic hepatitis C virus NS3/4A protease inhibitor voxilaprevir (GS-9857): A component of Vosevi®. *Bioorg. Med. Chem. Lett.* **2019**, *29*, 2428-2436, doi:https://doi.org/10.1016/j.bmcl.2019.03.037.
36. Aloup, J.-C.; Audiau, F.; Barreau, M.; Damour, D.; Genevois-Borella, A.; Jimonet, P.; Mignani, S.; Ribeill, Y. Preparation of imidazo[1,2-a]indeno[1,2-e]pyrazine-2-carboxylates as AMPA and NMDA receptor antagonists. WO9602544A1, 1996.
37. Aloup, J.-c.; Bouquerel, J.; Damour, D.; Hardy, J.-c.; Mignani, S. 2-Substituted 5H,10H-imidazo[1,2-a]indeno[1,2-e]pyrazin-4-ones, useful as AMPA and NMDA receptor antagonists, their preparation, and drugs containing them. WO9725326A1, 1997.

38. Bauer, L.; Nambury, C.N.V.; Bell, C.L. Studies in the chemistry of 3- and 5-isoxazolones. *Tetrahedron* **1964**, *20*, 165-171, doi:https://doi.org/10.1016/S0040-4020(01)93204-1.
39. Sarabia, F.; Sánchez-Ruiz, A.; Chammaa, S. Stereoselective synthesis of E-64 and related cysteine proteases inhibitors from 2,3-epoxyamides. *Biorg. Med. Chem.* **2005**, *13*, 1691-1705, doi:https://doi.org/10.1016/j.bmc.2004.12.018.
40. Vedadi, M.; Niesen, F.H.; Allali-Hassani, A.; Fedorov, O.Y.; Finerty, P.J., Jr.; Wasney, G.A.; Yeung, R.; Arrowsmith, C.; Ball, L.J.; Berglund, H., et al. Chemical screening methods to identify ligands that promote protein stability, protein crystallization, and structure determination. *Proc Natl Acad Sci U S A* **2006**, *103*, 15835-15840, doi:10.1073/pnas.0605224103.
41. Senisterra, G.A.; Markin, E.; Yamazaki, K.; Hui, R.; Vedadi, M.; Awrey, D.E. Screening for ligands using a generic and high-throughput light-scattering-based assay. *J. Biomol. Screen.* **2006**, *11*, 940-948.
42. Shahul Hameed, U.; Haider, I.; Jamil, M.; Kountche, B.A.; Guo, X.; Zarban, R.A.; Kim, D.; Al-Babili, S.; Arold, S.T. Structural basis for specific inhibition of the highly sensitive ShHTL7 receptor. *EMBO Rep* **2018**, *19*, doi:10.15252/embr.201745619.
43. Hamill, P.; Jean, F. Enzymatic Characterization of Membrane-Associated Hepatitis C Virus NS3-4A Heterocomplex Serine Protease Activity Expressed in Human Cells. *Biochemistry* **2005**, *44*, 6586-6596, doi:10.1021/bi047408j.
44. Vora, J.; Patel, S.; Athar, M.; Sinha, S.; Chhabria, M.T.; Jha, P.C.; Shrivastava, N. Pharmacophore modeling, molecular docking and molecular dynamics simulation for screening and identifying anti-dengue phytocompounds. *J. Biomol. Struct. Dyn.* **2019**, 10.1080/07391102.2019.1615002, 1-15, doi:10.1080/07391102.2019.1615002.
45. Pérez-Benito, L.; Keränen, H.; van Vlijmen, H.; Tresadern, G. Predicting Binding Free Energies of PDE2 Inhibitors. The Difficulties of Protein Conformation. *Sci. Rep.* **2018**, *8*, 4883, doi:10.1038/s41598-018-23039-5.
46. Cummings, M.D.; Lindberg, J.; Lin, T.I.; de Kock, H.; Lenz, O.; Lilja, E.; Fellander, S.; Baraznenok, V.; Nystrom, S.; Nilsson, M., et al. Induced-fit binding of the macrocyclic noncovalent inhibitor TMC435 to its HCV NS3/NS4A protease target. *Angew. Chem. Int. Ed. Engl.* **2010**, *49*, 1652-1655, doi:10.1002/anie.200906696.
47. Bennett, F.; Huang, Y.; Hendrata, S.; Lovey, R.; Bogen, S.L.; Pan, W.; Guo, Z.; Prongay, A.; Chen, K.X.; Arasappan, A., et al. The introduction of P4 substituted 1-methylcyclohexyl groups into Boceprevir: a change in direction in the search for a second generation HCV NS3 protease inhibitor. *Bioorg. Med. Chem. Lett.* **2010**, *20*, 2617-2621, doi:10.1016/j.bmcl.2010.02.063.
48. Prongay, A.J.; Guo, Z.; Yao, N.; Pichardo, J.; Fischmann, T.; Strickland, C.; Myers, J., Jr.; Weber, P.C.; Beyer, B.M.; Ingram, R., et al. Discovery of the HCV NS3/4A protease inhibitor (1R,5S)-N-[3-amino-1-(cyclobutylmethyl)-2,3-dioxopropyl]-3-[2(S)-[[[(1,1-dimethylethyl)amino]carbonyl]amino]-3,3-dimethyl-1-oxobutyl]-6,6-dimethyl-3-azabicyclo[3.1.0]hexan-2(S)-carboxamide (Sch 503034) II. Key steps in structure-based optimization. *J Med Chem* **2007**, *50*, 2310-2318, doi:10.1021/jm060173k.

49. Gomaa, A.; Allam, N.; Elsharkway, A.; El Kassas, M.; Waked, I. Hepatitis C infection in Egypt: prevalence, impact and management strategies. *Hepatic Medicine : Evidence and Research* **2017**, *9*, 17-25, doi:10.2147/HMER.S113681.
50. Mohamoud, Y.A.; Riome, S.; Abu-Raddad, L.J. Epidemiology of hepatitis C virus in the Arabian Gulf countries: Systematic review and meta-analysis of prevalence. *Int. J. Infect. Dis.* **2016**, *46*, 116-125, doi:https://doi.org/10.1016/j.ijid.2016.03.012.
51. Massariol, M.-J.; Zhao, S.; Marquis, M.; Thibeault, D.; White, P.W. Protease and helicase activities of hepatitis C virus genotype 4, 5, and 6 NS3–NS4A proteins. *Biochem. Biophys. Res. Commun.* **2010**, *391*, 692-697, doi:https://doi.org/10.1016/j.bbrc.2009.11.122.
52. Bawazir, A.; AlGusheri, F.; Jradi, H.; AlBalwi, M.; Abdel-Gader, A.-G. Hepatitis C virus genotypes in Saudi Arabia: a future prediction and laboratory profile. *Virology journal* **2017**, *14*, 208-208, doi:10.1186/s12985-017-0873-7.
53. Madhavi Sastry, G.; Adzhigirey, M.; Day, T.; Annabhimoju, R.; Sherman, W. Protein and ligand preparation: parameters, protocols, and influence on virtual screening enrichments. *J. Comput.-Aided Mol. Des.* **2013**, *27*, 221-234, doi:10.1007/s10822-013-9644-8.
54. Roos, K.; Wu, C.; Damm, W.; Reboul, M.; Stevenson, J.M.; Lu, C.; Dahlgren, M.K.; Mondal, S.; Chen, W.; Wang, L., et al. OPLS3e: Extending Force Field Coverage for Drug-Like Small Molecules. *J. Chem. Theory Comput.* **2019**, *15*, 1863-1874, doi:10.1021/acs.jctc.8b01026.